THE NUMERICAL MODELLING OF TRANSFORMATION INDUCED PLASTICITY IN THE DEEP DRAWING OF STAINLESS STEEL

by

J D B Ward

BSc Eng (Mechanical)

Department of Mechanical Engineering

University of Cape Town

A thesis submitted in partial fulfilment of the requirements for the degree of Master of Science in Engineering.

December 1993

Declaration

I hereby declare that the modelling, calculations and results presented in this thesis are essentially my own work and that no part of this work has been submitted for a degree at any other university.

Douglas Ward
December 1993

Acknowledgements

I would like to thank the following people for their assistance in completing this work:

Dr Colin Mercer[1] for his guidance in the initial stages of this study.

Dr Greg Mitchell[1] for his assistance with many problems.

Dr Rob Knutsen[2] for providing assistance in the understanding of the material behaviour and Mr Mandla Sibanda[2] for supplying details of deep drawing tests conducted in the Materials Engineering Department.

Prof. John Martin[1] for supervising this thesis.

[1] FRD/UCT Centre for Research in Computational and Applied Mechanics
[2] Materials Engineering Department, University of Cape Town

Abstract

Sheet metal forming processes are an important part of many manufacturing operations today. The numerical simulation of these processes has become an important aspect in the design of the processes and in the understanding of the material forming itself. This thesis document describes the development and formulation of a material model which was used in the numerical simulation of deep drawing problems.

The purpose of the material model was to predict the formation of martensite during the plastic straining of metastable austenitic stainless steel and the effect of the martensite formation on the plasticity of the steel. The model was developed from existing work as a modified von Mises isotropic hardening elastic-plastic algorithm. The algorithm was implemented as the subroutine UMAT in the finite element program ABAQUS.

Finite element simulations employing the material model were performed on two axisymmetric deep drawing examples. The finite element analysis was performed as a coupled displacement-temperature analysis.

The simulations produced results which predicted the distribution of various material state variables such as the volume fraction of martensite, plastic strain, yield stress and temperature in the formed component.

The results were consistent with what is intuitively expected from the physics of the problem. They were able to explain phenomena observed in physical tests such as the location of failures in the formed components and the occurrence of delayed cracking.

It is concluded that the model was successful in providing qualitative information on the distribution of martensite in components formed by deep drawing. These predictions were for a broad range of stainless steel behaviour. However, extensions to the model are required to be able to make accurate quantitative predictions on the formation of martensite in specific materials.

Table of Contents

List of Illustrations

List of Tables

Nomenclature and Notation

Roman

$\underline{\underline{D}}^e$	Elastic constitutive tensor for a homogeneous isotropic material
D, p	Rate dependency parameters
$\bar{e}^{pl}$	Equivalent plastic strain
$\underline{e}, \underline{e}^{el}, \underline{e}^{pl}$	Total, elastic and plastic deviatoric strain tensors
G	Shear modulus
H	Derivative of yield stress with respect to plastic strain
$\underline{I}$	Identity tensor
$\underline{n}$	Tensor of plastic flow direction
q	Invariant form of deviatoric stress, surface heat flux
q^e	Invariant form of elastic predictor deviatoric stress
r	Internal heat flux
r^{pl}	Plastic heat generation rate
$\underline{S}$	Deviatoric stress tensor
$\underline{S}^E$	Deviatoric elastic predictor stress tensor
t	Time
U	Internal energy
$\underline{u}$	Displacement vector
V_a, V_m	Volume fraction of austenite and martensite
Y	Derivative of yield stress with respect to temperature

Greek

$\bar{\sigma}_o$	Initial yield stress
$\bar{\sigma}$	Current yield stress
$\bar{\sigma}_{st}$	Static yield stress
$\bar{\sigma}_a, \bar{\sigma}_m$	Yield stress of austenite and martensite
$\underline{\sigma}$	Stress tensor
$\underline{\sigma}^E$	Elastic predictor stress tensor
$\underline{\varepsilon}$	Strain tensor
η	Fraction of plastic work converted to heat
θ	Temperature

ρ	Density
$\mathfrak{I}_{ijkl}$	Fourth order unit tensor
δ_{ij}	Kronecker delta

Tensor Notation

Tensor quantities are denoted by the following:

$\underline{T}$ for a second order tensor

$\underline{\underline{T}}$ for a fourth order tensor

The tensor product is denoted by: $\underline{T}:\underline{T}$

In component form this is given by the summation: $T_{ij}T_{ij}$

Vector Notation

In certain cases, vector notation is used. This is clearly indicated in the text where the vectors are denoted by: $\underline{V}$

Chapter 1
INTRODUCTION

1.1 Background

Metal forming in its different guises is an important aspect of many engineering processes today: hot-rolling, forging, extrusion, sheet stamping and deep drawing to name a few. In particular, sheet metal forming plays an important role in the manufacturing of products which affect our lives daily: e.g. car body parts, cooking utensils and beverage containers. The large plastic deformation common to most metal forming processes makes the design of these processes a difficult and often artful procedure. Hence a large amount of effort world-wide, in the form of numerical simulations, is concentrated on providing information to aid the design process and contribute to the understanding of metal processing in general.

1.1.1 Sheet Metal Forming

The term sheet metal forming refers to several different processes, each of which has certain characteristics with respect to the type of deformation processes that take place. These are chiefly deep drawing, stamping and various forms of hydraulic forming. In deep drawing the metal blank is drawn into the die by the tool or punch. This type of forming operation involves the stretching, compression and bending of the metal blank. In stamping operations the blank is not drawn into the die but is simply pressed into it by the punch. Deformation is mainly by stretching but can involve bending in the case of more complex formed parts. Hydraulic forming involves the stretching of the blank into the die by hydraulic pressure. Stretching is the main form of deformation in this type of process as well.

In each of the sheet forming processes described above, certain types of imperfections can occur in the formed part. These imperfections or defects can be specific to the type of forming process and their occurrence is dependent on certain factors (such as friction and ductility) governing the deformation modes described above. They can usually be classed as one of either wrinkling, tearing, earing or springback.

Wrinkling is specific to deep drawing operations and is characterised by the buckling of the sheet in areas of high radial compressive stress in the plane of the sheet. It can occur when the hold-down force of the blank holder and die is too small. This lack of restraint allows the sheet to be too readily drawn into the die with consequent high in-plane compressive stresses occurring in the radial direction. Wrinkling can, in some cases, be tolerated or removed. In

certain cases, however, it may be excessive and undesirable for visual or functional reasons. It is thus important to be able to predict the occurrence of wrinkling and find possible ways of avoiding it. Ameziane-Hassani and Neale [1] established what they call 'Wrinkling Limit Curves' (WLC) for sheet metal forming. These curves represent combinations of the critical principal stresses at which wrinkling occurs. Their investigation was based on a bifurcation analysis for plastic buckling. A finite element scheme was developed to perform the analysis which included the effects of material properties, sheet geometry and initial geometric imperfections. Predictions of the occurrence of wrinkling were thus provided for a wide range of sheet metal forming situations.

Tearing is common to all forms of sheet forming and is characterised by the rupturing of the sheet in areas of high tensile strain. This type of defect is caused by an excessive hold-down force in deep drawing operations or simply by the excessive stretching of the blank in general and has been well researched to date. Keeler [2] produced empirical curves (known as Forming Limit Curves) predicting the critical strains for certain input conditions such as sheet thickness and material properties. In this experimental work, failure of the metal sheet is defined as either tearing or necking (strain localisation just prior to tearing itself): whichever is detectable first. It has been found that lubrication conditions play an important role in the occurrence of tearing. For example an over lubricated punch/blank interface can result in insufficient material being drawn from the flange and consequent tearing taking place.

Earing is specific to deep drawing operations and is caused by the anisotropic nature of the material properties. It is visible as the irregular shape of the flange of the formed component, e.g. in an axisymmetric component the flange would not be circular. The occurrence of earing defects in deep drawing operations is caused by uneven drawing of the blank material from the flange. This could be caused by two possible factors: material anisotropy and friction conditions between the blank holder and the blank (related to the blank holder force). However, Chung and Shah [3] show in their results for a deep drawing analysis that the effect of blank-holder force and coefficient of friction chosen was insignificant in the prediction of earing compared to the effect of material anisotropy.

Springback is simply the elastic unloading of the formed part after the withdrawing of the punch. This phenomenon is unavoidable and can result in an unacceptable change in part shape. The only solution to this problem is the design of a punch or forming tool and die to produce the correct part shape after unloading. Karafillis and Boyce [4] produced a design algorithm which used the finite element method to predict springback. The algorithm involved an iterative procedure to arrive at tool designs which would produce the correct part shape after unloading.

1.1.2 Transformation Induced Plasticity

In addition to the possible forming problems described above, the deep drawing of certain stainless steels can give rise to further problems as a result of the phenomenon known as transformation induced plasticity. During plastic straining, metastable austenitic stainless steels, and in particular type 304, exhibit a change in phase from austenite to martensite. The extent of this phase transformation is influenced by the level of plastic strain and the temperature of the material. The formation of martensite can have a strengthening effect on certain steels which is manifested as an increase in both the yield stress and the amount of plastic strain possible before rupture. This is illustrated in Figure 1 below. It is this strengthening effect as a result of martensite formation that is known as transformation induced plasticity.

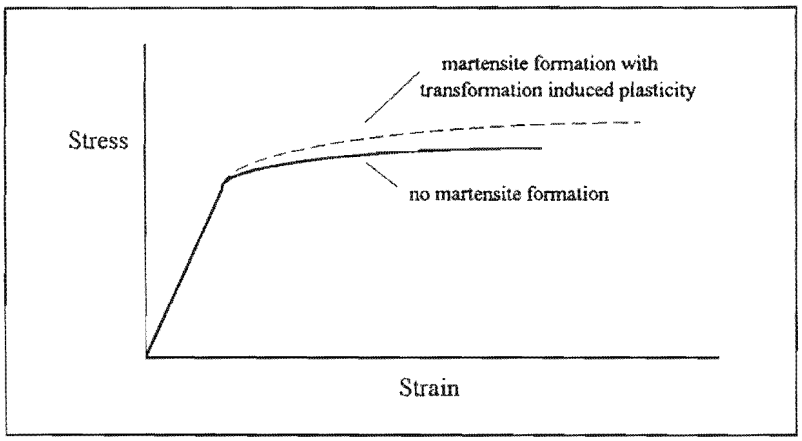

Figure 1. Change in yield stress as a result of transformation induced plasticity.

Ludwigson and Berger [14] present stress strain relations for metastable austenitic stainless steels including transformation induced plasticity effects. Their results show the strengthening effect that the evolution of martensite can have on certain steels.

The localised formation of martensite as a result of plastic deformation can result in cracking in formed components after the drawing process is complete, although the exact reasons for this cracking are not yet understood. The occurrence of this phenomenon is, however, sensitive to small changes in the chemical composition of the steel as reported by Knutsen [13].

The occurrence of transformation induced plasticity in deep drawing lends itself to investigation by the finite element method. This is due to the complicated distribution of plastic strain in an article undergoing deep drawing. In addition, the temperature distribution

(on which the transformation is dependent) is largely influenced by factors such as frictional heat generation which the finite element method is capable of modelling with reasonable accuracy. Material models specifically aimed at predicting the occurrence of transformation induced plasticity can also be readily implemented in existing finite element codes.

Stringfellow and Parks [15] present the mathematical formulation of a rate dependent material model that handles phase transformations as a function of plastic strain and temperature in multiphase materials. Their model was implemented in a user-material subroutine in ABAQUS [12]. Model predictions for uniaxial tension tests were compared with data from physical tests. Stringfellow, Parks and Olson [16] present a slightly different material model in which martensite formation is a function of stress state as well as plastic strain and temperature. A far simpler material model was implemented by Shinagawa *et al* [17] and applied directly to an axisymmetric sheet forming example. This model was based on the decomposition of the yield stress into a function depending on the volume fraction of martensite and the yield stresses of the two separate phases. Their results of forming simulations successfully predicted the distribution of martensite in an article formed from 304 stainless steel.

1.1.3 Finite Element Simulation of Sheet Metal Forming

The finite element simulation of sheet metal forming operations is typically carried out to achieve two main goals. Firstly it aims to predict the occurrence of defects without the need for physical experimentation, and secondly, it aims to provide sufficient information for avoiding these defects in the design and manufacture of sheet metal components.

The complexity of the physical processes governing sheet metal forming poses severe challenges in their simulation by the finite element method. The first problem is the choice of element type. Element types suitable for sheet metal forming analyses are 3-D continuum elements, 2-D axisymmetric continuum elements, and shell and membrane elements. The choice of element type influences the speed of the solution and also determines which of the relevant deformation processes will be accurately modelled. A balance must be sought between solution efficiency and solution accuracy; efficiency being the solution speed and accuracy being determined by whether or not the relevant deformation processes are being adequately modelled.

The decision whether to use continuum or specialised elements depends on the importance of through thickness stresses in the plate material. Rebelo *et al* [6] showed that for deep drawing operations and for other thin sheet forming operations where contact is effectively one-sided,

through thickness stresses are not important. However, Karafillis and Boyce [4] point out that for forming operations in which the die is not bottomless, as in stamping operations (for complicated part shapes such as automobile panels), the two sided contact conditions introduce through thickness stresses which require the use of continuum elements.

Considering the use of specialised elements, an important aspect of many forming operations, especially deep drawing, is the effect of bending on the deformation of the metal blank. This is particularly important in the prediction of springback. Since the use of membrane elements over shell elements is preferred for solution efficiency and since membrane elements do not model bending a decision has to be made on which of the element types is most appropriate. Wang and Tang [8] provide a comparison of the performance of shell and membrane elements. They found that the use of shell elements provides a small correction over the use of membrane elements in deep drawing operations. Bellet *et al* [9] found that the membrane approximation is sufficient for applications in which the ratio of the radius of curvature of the die or punch to the blank thickness is larger than 5. This means that membrane elements are excluded from applications of deep drawing with drawbeads. Yang *et al* [10] also provide a comparison of membrane and shell elements. They found that there was good agreement in the prediction of the punch load-displacement curve for both analyses. However in the prediction of strain distribution they found that bending effects were important and that shell elements gave better results.

The second major problem in the finite element simulation is the modelling of contact and friction conditions between the die and blank holder and the blank. These phenomena are one of the most difficult aspects of sheet metal forming to model accurately and efficiently. Of several recognised methods that have been developed the two most suitable are known as the penalty method and the Lagrange multiplier method.

Owen and Peric [11] present a detailed description of a scheme for handling contact and friction in three dimensions based on the penalty method. The penalty method was chosen in the anticipation that good results can be obtained for situations not involving high normal forces (as is the case in sheet metal forming). Friction conditions are modelled on the same lines as classical elastoplasticity.

Rebelo *et al* [6] present a detailed description of a contact and friction model which forms part of the basis for a commercial code [12]. Their model is based on the use of Lagrange multipliers to enforce contact and a surface constitutive model based on an elastic-plastic analogy is used with a limit on the maximum allowable shear stress before sliding takes place.

Karafillis [5] implemented a similar contact and friction model in the user subroutine facility in ABAQUS using the penalty method for contact. His model is also based on an elastic-plastic type surface constitutive model with Coulomb friction. A yield curve represents the limit of elastic slip ('sticking') before plastic slip ('sliding') takes place. A relationship between normal force and the elastic 'sticking stiffness' prior to slip reduces the non-linearity of the friction description and so produces a scheme with improved convergence characteristics.

In addition to the above problems (pertaining to the finite element model itself) there is the additional complexity of modelling the material behaviour. In particular, material models may have to account for the anisotropic nature of the properties of sheet materials - especially in the prediction of earing defects and strain distribution.

Most of the analyses performed in the literature, including those discussed above, assume material isotropy in the plane of the sheet blank and anisotropy normal to this plane. Hill's anisotropic yield criterion is generally used in these models. However, if a complete description of the material deformation is to be obtained anisotropy in the plane of the metal blank must also be allowed for. Chung and Shah [3] present an analysis which makes use of a more recent anisotropy criterion by Barlat [20]. They implemented this model in the user subroutine facility in the code ABAQUS and analysed both the hydraulic forming and the deep drawing of a material of fairly small anisotropy. Their results for hydraulic bulge forming showed little influence of the anisotropy of the material on the deformations predicted. However, in the deep drawing analysis good agreement was obtained with experimental data in the prediction of the occurrence of earing.

1.2 Objectives

The objectives of this study were:

1. To formulate a material constitutive model (based on existing work [17]) for 304 stainless steel that predicts the occurrence of transformation induced plasticity and includes its effects in the material behaviour;

2. To perform finite element simulations (employing the material model) of a simple deep drawing example in order to investigate certain aspects of the model developed. The results of these simulations would be used to verify the assumptions made; and

3. To perform finite element simulations of an actual deep drawing problem and illustrate the usefulness of the material model in explaining certain observed phenomena.

1.3 Scope and Limitations

The model developed in this study was intended to predict the occurrence of transformation induced plasticity in 304 stainless steel: i.e. the model predicts only enhanced plasticity as a result of martensite evolution. It should be noted that substantial differences in material properties exist between different grades of the same type of steel, especially with regard to the tendency to undergo transformation induced plasticity. The material model presented here makes no attempt to distinguish between these different properties and is intended to provide a broad approximation of the behaviour of metastable austenitic stainless steels which exhibit transformation induced plasticity effects.

Evaluation of the results obtained from the use of the model is severely limited by the lack of specific material property data with which to make quantitative comparisons. Any conclusions arrived at concerning the applicability of the model are thus based on qualitative comparisons and observations only.

Chapter 2
THE MATERIAL MODEL

The purpose of the material model developed in this study was firstly to predict the formation of martensite in the material being formed and secondly to take into account the change in the plasticity of the material as a result of this martensite formation. The model is based on von Mises elastoplasticity with a uniaxial yield stress defined according to the current volume fraction of martensite in the material. This yield stress is used to impose a yield condition on which the plasticity calculations are based.

2.1 Elastoplasticity

The material behaviour is assumed to be entirely elastic until some condition for yield is met. The elastic stress-strain relationship is given by

$$\underline{\sigma} = \underline{\underline{D}}^{e} \underline{\varepsilon}^{el} \qquad 2.1.1$$

where $\underline{\sigma}$ and $\underline{\varepsilon}^{el}$ are the stress and elastic strain tensors, respectively, and $\underline{\underline{D}}^{e}$ is the standard elastic constitutive tensor for a homogeneous isotropic material. Once yield has occurred an additive decomposition of the strain rate into elastic and plastic components is assumed:

$$\dot{\underline{\varepsilon}} = \dot{\underline{\varepsilon}}^{el} + \dot{\underline{\varepsilon}}^{pl}$$

This can be written in integrated form as:

$$\underline{\varepsilon} = \underline{\varepsilon}^{el} + \underline{\varepsilon}^{pl} \qquad 2.1.2$$

Now, deviatoric quantities of stress and strain are defined by

$$\underline{S} = \underline{\sigma} - \frac{1}{3} trace(\underline{\sigma}) \underline{I} \quad \text{for stress}$$

and

$$\underline{e} = \underline{\varepsilon} - \frac{1}{3} trace(\underline{\varepsilon}) \underline{I} \quad \text{for strain,}$$

where $\underline{I}$ is the identity tensor. An additive strain decomposition is also assumed for deviatoric strain, hence the stress-strain relationship for deviatoric components is given by

$$\underline{S} = 2G\underline{e}^{el} \qquad 2.1.3$$

where G is the shear modulus. Note that, since a von Mises plasticity theory is used, all plastic deformation is deviatoric (i.e. volumetric behaviour is purely elastic).

2.2 Plasticity Laws

2.2.1 Yield Condition

In the rate dependent plasticity model an initial condition for yielding is defined by

$$q > \bar{\sigma}_o \qquad 2.2.1.1$$

where $$q = \sqrt{\frac{3}{2}\underline{S}:\underline{S}} \qquad 2.2.1.2$$

and $\bar{\sigma}_o$ is the initial rate dependent uniaxial yield stress (i.e. for no plastic strain having occurred).

Once yield is detected the material is assumed to satisfy the yield condition:

$$q = \bar{\sigma} \qquad 2.2.1.3$$

where $$\bar{\sigma} = \bar{\sigma}(\bar{e}^{pl}, \dot{\bar{e}}^{pl}, \theta)$$

where $\bar{e}^{pl}$ is the equivalent plastic strain, $\dot{\bar{e}}^{pl}$ is the plastic strain rate and θ is the temperature.

2.2.2 Plastic Flow Rule

The deviatoric plastic strain rate is expressed in terms of the equivalent plastic strain rate by the plastic flow rule. This is given by

$$\underline{\dot{e}}^{pl} = \dot{\bar{e}}^{pl}\frac{\partial q}{\partial \underline{S}} \qquad 2.2.2.1$$

2.3 Strain Rate Dependence

The strain rate dependence of the yield stress is modelled by the following equation [12]

$$\bar{\sigma} = \bar{\sigma}_{st}\left(\left(\frac{\dot{\bar{e}}^{pl}}{D}\right)^{\frac{1}{p}} + 1\right) \qquad 2.3.1$$

where $\bar{\sigma}_{st}$ is the static yield stress and D and p are parameters which determine the degree of rate dependence of the material. The choice of these parameters is difficult. Experimental

work on rate dependency rarely yields results which can be used to determine accurate values. However numerical comparisons between this equation and a strain rate function [17] have yielded approximate values for these constants. This point will be dealt with in more detail in Chapter 5.

2.4 Static Yield Stress

The static yield stress $\overline{\sigma}_{st}$ is assumed to be composed of the yield stresses of the two separate phases. Hence a yield stress decomposition can be written [17] which expresses the total static yield stress in terms of the yield stresses of the two phases and their respective volume fractions:

$$\overline{\sigma}_{st} = \overline{\sigma}_a V_a + \overline{\sigma}_m V_m^Q \qquad 2.4.1$$

where the subscripts a and m denote the austenite and martensite phases respectively, and Q is the martensitic strengthening index proposed by Ludwigson [14] with a value of 0.85. It is important to note that equation 2.4.1 predicts a strengthening effect as a result of martensite formation in the material. Certain stainless steels exhibit weakening as a result of martensite evolution and are hence excluded from being modelled in this way.

The yield stress of the austenitic phase is approximated as the yield stress of 316 stainless steel. This is a stable austenitic stainless steel exhibiting no transformation induced plasticity effects and hence no martensite formation. Shinagawa *et al* [17] propose a function to express the yield stress of the austenitic phase, $\overline{\sigma}_a$, in terms of strain, strain rate and temperature. This is shown in Appendix B.2. The function used here is a simplified version of the one presented in [17]. The reasoning behind this is that a function of too great a complexity is attempting to be too accurate within the approximations of the broader finite element analysis. The simplified function used is independent of strain rate and linearly dependent on temperature: its derivation is explained in Appendix B.3. It is given by:

$$\overline{\sigma}_a = 245 - 0.45\theta + 1788\overline{e}^{pl} \qquad \left(\overline{e}^{pl} < 0.129\right) \qquad 2.4.2$$

$$\overline{\sigma}_a = (245 - 0.45\theta)\left(\frac{0.779}{\overline{e}^{pl} + 0.65}\right)^{0.6} + 1788\overline{e}^{pl} \qquad \left(\overline{e}^{pl} \geq 0.129\right) \qquad 2.4.3$$

where θ is the material temperature in degrees Celsius, $\overline{e}^{pl}$ the equivalent plastic strain, and the yield stress is given in MPa.

The yield stress of the martensitic phase is assumed to be a constant: $\overline{\sigma}_m$ = 1591 MPa [17].

2.5 Martensite Formation

The following expression [17] was used to model the evolution of martensite as a function of temperature, existing martensite content and change in plastic strain:

$$\frac{dV_m}{d\bar{e}^{pl}} = k(V_m + s)(f - V_m) \qquad 2.5.1$$

where V_m is the current volume fraction of martensite and k, s and f are temperature dependent parameters [17] given in Table 2.5. Linear interpolation is used to obtain continuous values for the parameters over the required range of temperature.

Table 2.5 Temperature dependent parameters k, s and f.

T (°C)	k	s	f
0	0	1	1
20	6.5	0.055	0.64
30	11	0.02	0.46
40	17	0.003	0.33
50	31	0	0.22
70	1006	0	0.03
100	2626	0	0

Equation 2.5.1 can be integrated to give the volume fraction of martensite for a given level of plastic strain and temperature as shown in Figure 2.1. In the numerical implementation this is done using a backward Euler method.

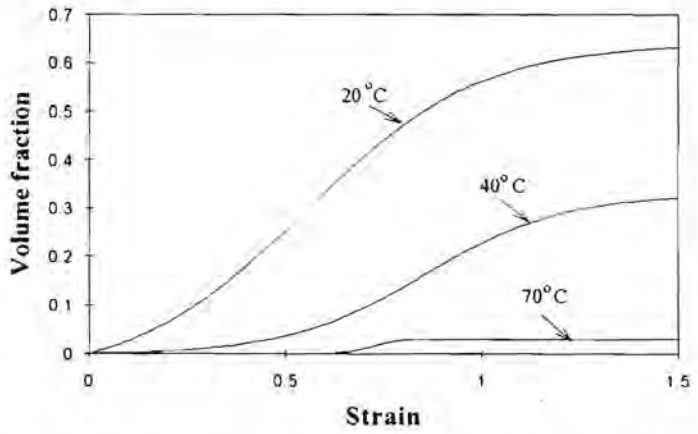

Figure 2.1 Volume fraction of Martensite versus Strain and Temperature.

2.6 Temperature Effects

Martensite formation is strongly dependent on temperature. Therefore, to complete the material model definition, heat generation due to plastic work must be defined. This was modelled by the following expression

$$r^{pl} = \eta \dot{\bar{e}}^{pl} \bar{\sigma} \qquad 2.6.1$$

where r^{pl} is the heat flux per unit volume into the material and η is the fraction of plastic dissipation energy which is assumed to be converted to heat.

Straining of the material due to thermal expansion was ignored. It was assumed that these strains would be very small compared to the large plastic strains dominant in the process.

Chapter 3
MATERIAL COMPUTATIONS

The material behaviour model described in Chapter 2 was implemented as user subroutine UMAT in the finite element program ABAQUS and is given in Appendix C.1. The subroutine was written for application in plane strain and axisymmetric cases.

3.1 Computation Procedure

For each increment the program ABAQUS provides the user subroutine with the current states of stress and strain, the value of state variables (such as plastic strain and volume fraction of martensite) and the increment of total strain. The calculation of the stress and state variables at the end of the increment is required. ABAQUS uses a Newton-Raphson solution scheme hence the calculation of the consistent modulus used in this scheme is also required. The following basic procedure is executed in performing these calculations at each integration point for each increment:

1. *Elastic Predictor*: the stress state is predicted as if deformation is entirely elastic in the current increment.

2. *Yield Condition*: the stress state calculated in 1. is checked against the condition for yield (Section 2.2.1). If yield has not occurred then the material state calculated in 1. is returned for that increment.

3. *Plasticity Algorithm*: in the case of yield being detected the von Mises plasticity calculations are performed to determine the material state variables including the volume fraction of martensite.

4. *Consistent Modulus*: the terms for the consistent modulus required in the iterative solution of the global finite element equations are calculated.

Note: all quantities given are those at the end of the current increment unless otherwise stated.

3.2 Elastic Predictor

The elastic predictor stress state for the increment is calculated as shown in the following equation

$$\underline{\sigma}^E = \underline{\sigma}|_t + \underline{\underline{D}}^e \Delta \underline{\varepsilon} \qquad 3.2.1$$

where $\underline{\sigma}^E$ is the tensor of elastic predictor stress, $\underline{\sigma}|_t$ is the stress state at the start of the increment, $\underline{\underline{D}}^e$ is the elastic constitutive matrix and $\Delta \underline{\varepsilon}$ is the tensor of strain increments. The deviatoric elastic predictor stress state is obtained by

$$\underline{S}^E = \underline{\sigma}^E - \frac{1}{3} trace\left(\underline{\sigma}^E\right) \underline{I} \qquad 3.2.2$$

where $\underline{I}$ is the identity tensor.

3.3 Von Mises Plasticity Algorithm

The deviatoric elastic predictor stress state calculated in Section 3.2 is checked against the condition for yield given by expression 2.2.1:

$$\sqrt{\frac{3}{2} \underline{S}^E : \underline{S}^E} > \overline{\sigma}_o$$

where $\overline{\sigma}_o$ is the initial yield stress if yield has not yet occurred or the yield stress, $\overline{\sigma}|_t$, from the previous increment if yield has already occurred at the material point. If yield is detected the stress state must be returned to the yield surface to satisfy the yield condition

$$q = \overline{\sigma} \qquad 3.3.1$$

where $$q = \sqrt{\frac{3}{2} \underline{S} : \underline{S}} \qquad 3.3.2$$

and $$\overline{\sigma} = \overline{\sigma}(\overline{e}^{pl}, \dot{\overline{e}}^{pl}, \theta) \qquad 3.3.3$$

$\overline{\sigma}$ is the uniaxial yield stress which is described in detail in Chapter 2, $\overline{e}^{pl}$ the equivalent plastic strain and θ is the temperature.

Now the plastic flow rule defined in Section 2.2.2 is integrated using the backward Euler method to give

$$\Delta \underline{e}^{pl} = \Delta \overline{e}^{pl} \underline{n} \qquad 3.3.4$$

where $$\underline{n} = \frac{3\underline{S}}{2q} \qquad 3.3.5$$

This is combined with equation 2.1.3 to give

$$\underline{S} = 2G(\underline{e}^{el}\big|_t + \Delta\underline{e} - \Delta\bar{e}^{pl}\underline{n}) \qquad 3.3.6$$

where $\underline{e}^{el}\big|_t$ is the deviatoric elastic strain at the start of the increment and $\Delta\underline{e}$ is the increment of total deviatoric strain. This expression now yields the following equation for the updated deviatoric stresses:

$$\underline{S} = \frac{2G}{(1+\frac{3G}{q}\Delta\bar{e}^{pl})}\hat{\underline{e}} \qquad 3.3.7$$

where $$\hat{\underline{e}} = \underline{e}^{el}\big|_t + \Delta\underline{e} \qquad 3.3.8$$

and $\Delta\bar{e}^{pl}$ is the increment of equivalent plastic strain which is calculated from the iterative solution of the following expression for the yield condition:

$$G(2\tilde{e} - 3\Delta\bar{e}^{pl}) - \bar{\sigma} = 0 \qquad 3.3.9$$

where $$\tilde{e} = \sqrt{\frac{3}{2}\hat{\underline{e}}:\hat{\underline{e}}} \qquad 3.3.10$$

Equations 3.3.7 - 10 give the complete set of computations required to update the stress in an increment in which plastic deformation is detected. In practice, however, these equations are not used. Greater numerical accuracy is obtained by using the following [18]:

$$q^e - 3G\Delta\bar{e}^{pl} - \bar{\sigma} = 0 \qquad 3.3.11$$

where $$q^e = \sqrt{\frac{3}{2}\underline{S}^E:\underline{S}^E} \qquad 3.3.12$$

for the solution of $\Delta\bar{e}^{pl}$ and,

$$\underline{S} = \frac{2\bar{\sigma}\underline{n}}{3} \qquad 3.3.13$$

for updating the stress state where $\underline{n}$ is the plastic flow direction which must be calculated from the elastic predictor quantities since $\underline{S}$ is unknown:

$$\underline{n} = \frac{3\underline{S}^E}{2q^e} \qquad 3.3.14$$

Now to determine the value of $\bar{\sigma}$ used in equation 3.3.1 the volume fraction of martensite needs to be calculated. This is done by backward Euler integration of equation 2.5.1:

$$\Delta V_m = k(V_m|_t + s)(f - V_m|_t)\Delta\bar{e}^{pl} \qquad 3.3.15$$

where ΔV_m is the increment in the volume fraction of martensite, $V_m|_t$ is the volume fraction of martensite at the start of the increment and k, s and f are the temperature dependent parameters given in Table 2.1.

3.4 Plastic Heat Generation

The material subroutine was also required to calculate the heat generation due to plastic dissipation. ABAQUS [12] requires the calculation of the heat flux per unit volume at the material point which is given by equation 2.6.1. This was calculated numerically by the following expression

$$r^{pl} = \frac{1}{2\Delta t}\eta\Delta\bar{e}^{pl}(\hat{\sigma} + \bar{\sigma}) \qquad 3.4.1$$

where Δt is the increment time length, $\Delta\bar{e}^{pl}$ is the plastic strain increment, $\bar{\sigma}$ is the yield stress at the end of the increment given by

$$\bar{\sigma} = \bar{\sigma}_{st}\left(\left(\frac{\dot{\bar{e}}^{pl}}{D}\right)^{\frac{1}{p}} + 1\right)$$

where $\bar{\sigma}_{st}$ is the static yield stress at the end of the increment, and $\hat{\sigma}$ is given by

$$\hat{\sigma} = \bar{\sigma}_{st}|_t\left(\left(\frac{\dot{\bar{e}}^{pl}}{D}\right)^{\frac{1}{p}} + 1\right) \qquad 3.4.2$$

where $\bar{\sigma}_{st}|_t$ is the static yield stress at the start of the increment. η is the fraction of plastic dissipation energy which is assumed to be converted to heat; this is generally taken as 0.9.

3.5 Consistent Modulus

3.5.1 Basic Finite Element Equations

The large temperature changes occurring simultaneously with large strains in the type of problem to be analysed using this material model require the use of a coupled temperature-displacement formulation. This involves the simultaneous solution of the following governing equations: the force equilibrium equation

$$\int_V \underline{\sigma} dV + \int_S \underline{f} dS = 0 \qquad 3.5.1.1$$

where $\underline{f}$ is the surface traction and $\underline{\sigma}$ is the stress at a point in a body; and the thermal energy balance equation

$$\int_V \rho \dot{U} dV = \int_S q dS + \int_V r dV \qquad 3.5.1.2$$

where ρ is the density, $\dot{U}$ is the internal energy rate, q is the surface heat flux into the body and r is the internal heat flux per unit volume. S and V denote integrals over the surface and volume of the body, respectively.

The finite element equations are derived from the virtual work expression of equation 3.5.1.1:

$$F(\underline{u}, \theta, \delta\underline{u}) = \int_V \delta\underline{\varepsilon}^T \underline{\sigma} dV - \int_S \delta\underline{u}^T \underline{f} dS \qquad 3.5.1.3$$

where δ denotes virtual quantities and $\underline{u}$ is the vector of displacements; and the variational expression of equation 3.5.1.2 which is given by

$$Q(\underline{u}, \theta, \delta\theta) = \int_V \delta\theta \rho \dot{U} dV - \int_S \delta\theta q dS - \int_V \delta\theta r dV \qquad 3.5.1.4$$

Writing the above expressions using the Taylor Formula about quantities at n to first order and setting them to zero, an iterative solution scheme can be defined as:

$$F_n^j(\underline{u} + d\underline{u}, \theta + d\theta, \delta\underline{u}) = F_n^j(\underline{u}, \theta, \delta\underline{u}) + \frac{\partial F}{\partial \underline{u}}\Big|_n^j \partial\underline{u} + \frac{\partial F}{\partial \theta}\Big|_n^j \partial\theta = 0 \qquad 3.5.1.5$$

$$Q_n^j(\underline{u} + d\underline{u}, \theta + d\theta, \delta\theta) = Q_n^j(\underline{u}, \theta, \delta\theta) + \frac{\partial Q}{\partial \underline{u}}\Big|_n^j \partial\underline{u} + \frac{\partial Q}{\partial \theta}\Big|_n^j \partial\theta = 0 \qquad 3.5.1.6$$

where n denotes the value at the end of increment n and j denotes the value at iteration j.

Since $\delta\underline{u}$ and $\delta\theta$ are arbitrary the solution procedure defined by equations 3.5.1.5 and 3.5.1.6 can be combined to give the global set of finite element equations as follows:

$$\begin{bmatrix} \underline{\underline{K}}^{uu} \Big|_n^j & \underline{\underline{K}}^{u\theta} \Big|_n^j \\ \underline{\underline{K}}^{\theta u} \Big|_n^j & \underline{\underline{K}}^{\theta\theta} \Big|_n^j \end{bmatrix} \begin{pmatrix} d\underline{u}_n^j \\ d\underline{\theta}_n^j \end{pmatrix} = \begin{pmatrix} \underline{F}_n^j \\ \underline{Q}_n^j \end{pmatrix} \qquad 3.5.1.7$$

where $d\underline{u}_n^j$ and $d\underline{\theta}_n^j$ are the vectors of nodal displacement and temperature increments respectively, and

$$\underline{\underline{K}}^{uu} = \frac{\partial \underline{F}}{\partial \underline{u}} = \int_V \underline{\underline{B}}_u^T \underline{\underline{D}}^{\sigma\varepsilon} \underline{\underline{B}}_u dV$$

$$\underline{\underline{K}}^{u\theta} = \frac{\partial \underline{F}}{\partial \theta} = \int_V \underline{\underline{B}}_u^T \underline{D}^{\sigma\theta} \underline{B}_\theta dV$$

$$\underline{\underline{K}}^{\theta u} = \frac{\partial \underline{Q}}{\partial \underline{u}} = \int_V \underline{B}_\theta^T \underline{D}^{r\varepsilon} \underline{\underline{B}}_u dV$$

$$\underline{\underline{K}}^{\theta\theta} = \frac{\partial \underline{Q}}{\partial \theta} = \int_V \underline{B}_\theta^T D^{r\theta} \underline{B}_\theta dV$$

where $\underline{\underline{B}}_u$ is the matrix of interpolation functions for nodal displacements and $\underline{B}_\theta$ is the vector of interpolation functions for nodal temperatures. Now,

$$\underline{\underline{D}}^{\sigma\varepsilon} = \frac{\partial \underline{\sigma}}{\partial \underline{\varepsilon}}$$

$$\underline{D}^{\sigma\theta} = \frac{\partial \underline{\sigma}}{\partial \theta}$$

$$\underline{D}^{r\varepsilon} = -\frac{\partial r}{\partial \underline{\varepsilon}}$$

$$D^{r\theta} = -\frac{\partial r}{\partial \theta}$$

Here stress and strain are given as vectors. The terms D above are referred to as the Consistent Modulus. It should be noted that the stiffness matrix in equation 3.5.1.7 formed by the terms K above is strongly non-symmetric, thus necessitating the calculation of all its terms.

In this case $r = r^{pl}$ (plastic heat generation) defined by equation 3.4.1 For the purposes of implementation in ABAQUS and since $\underline{\sigma}$ and r^{pl} are defined by the material subroutine the following quantities need also to be computed by the material subroutine:

$$\frac{\partial \underline{\sigma}}{\partial \underline{\varepsilon}}, \text{ and } \frac{\partial \underline{\sigma}}{\partial \theta}$$

for the global force equilibrium equation, and:

$$\frac{\partial r^{pl}}{\partial \underline{\varepsilon}}, \text{ and } \frac{\partial r^{pl}}{\partial \theta}$$

for the global thermal energy balance equation.

3.5.2 Calculation of Terms for the Consistent Modulus

The terms for the consistent modulus are derived formally using tensor notation. However, in the numerical implementation they are treated as vectors and matrices. The terms for the global force equilibrium are obtained by taking variations of equations 3.3.3 and 3.3.7 - 10. See Appendix B.1 for derivations. These terms are given by [18]

$$\frac{\partial \underline{\sigma}}{\partial \underline{\varepsilon}} = Q\underline{\underline{\mathfrak{I}}} + (K - \frac{1}{3}Q)\underline{I}\,\underline{I} - R\underline{S}\,\underline{S} \qquad 3.5.2.1$$

where

$$Q = \frac{\bar{\sigma}}{\bar{e}} \qquad 3.5.2.2$$

$$R = \frac{9G}{2\bar{\sigma}\bar{e}}\left(\frac{1}{H+3G}\right)\left(1 - \frac{\Delta \bar{e}^{pl} H}{\bar{\sigma}}\right) \qquad 3.5.2.3$$

$$H = \frac{\partial \bar{\sigma}}{\partial \bar{e}^{pl}} \qquad 3.5.2.4$$

and

$$\frac{\partial \underline{\sigma}}{\partial \theta} = \frac{3G}{\bar{\sigma}(H+3G)} Y\underline{S} \qquad 3.5.2.5$$

where

$$Y = \frac{\partial \bar{\sigma}}{\partial \theta} \qquad 3.5.2.6$$

and $\underline{\underline{\mathfrak{I}}}$ is the 4th order unit tensor (in component form: $\mathfrak{I}_{ijkl} = \delta_{ik}\delta_{jl}$) and $\underline{I}$ is the identity tensor δ_{ij}, where δ_{ij} is the Kronecker delta. The values of H and Y are obtained by differentiating equations 2.3.1 and 2.4.1 - 3.

The thermal energy balance terms are obtained by differentiating equation 3.4.1 - this is done as follows: first we have

$$\frac{\partial r^{pl}}{\partial \underline{\varepsilon}} = \frac{\eta}{2\Delta t}\left[\frac{\partial \bar{e}^{pl}}{\partial \underline{\varepsilon}}(\hat{\sigma}+\bar{\sigma}) + \Delta \bar{e}^{pl}\left(\frac{\partial \hat{\sigma}}{\partial \bar{e}^{pl}} + \frac{\partial \bar{\sigma}}{\partial \bar{e}^{pl}}\right)\frac{\partial \bar{e}^{pl}}{\partial \underline{\varepsilon}}\right] \qquad 3.5.2.7$$

Now from equation 3.4.2, $\frac{\partial \hat{\sigma}}{\partial \bar{e}^{pl}} = \frac{\partial \hat{\sigma}}{\partial \dot{\bar{e}}^{pl}}\frac{\partial \dot{\bar{e}}^{pl}}{\partial \bar{e}^{pl}}$

So, $$\frac{\partial \hat{\sigma}}{\partial \bar{e}^{pl}} = \bar{\sigma}_{st}\big|_t \frac{1}{p\Delta \bar{e}^{pl}}\left(\frac{\dot{\bar{e}}^{pl}}{D}\right)^{\frac{1}{p}} \qquad 3.5.2.8$$

Substituting this into equation 3.5.2.7 and simplifying gives

$$\frac{\partial r^{pl}}{\partial \underline{\varepsilon}} = \frac{\eta}{2\Delta t}\frac{\partial \bar{e}^{pl}}{\partial \underline{\varepsilon}}\left(\hat{\sigma}+\bar{\sigma}+\Delta \bar{e}^{pl}H + \bar{\sigma}_{st}\big|_t B\right) \qquad 3.5.2.9$$

where $$B = \frac{1}{p}\left(\frac{\dot{\bar{e}}^{pl}}{D}\right)^{\frac{1}{p}} \qquad 3.5.2.10$$

Now, by the chain rule, $$\frac{\partial \bar{e}^{pl}}{\partial \underline{\varepsilon}} = \frac{\partial \bar{e}^{pl}}{\partial \bar{\sigma}}\frac{\partial \bar{\sigma}}{\partial \underline{S}} : \frac{\partial \underline{S}}{\partial \underline{\sigma}} : \frac{\partial \underline{\sigma}}{\partial \underline{\varepsilon}} \qquad 3.5.2.11$$

where $$\frac{\partial \bar{e}^{pl}}{\partial \bar{\sigma}} = \frac{1}{H} \qquad 3.5.2.12$$

$$\frac{\partial \bar{\sigma}}{\partial \underline{S}} = \underline{n} \qquad 3.5.2.13$$

and $$\frac{\partial \underline{S}}{\partial \underline{\sigma}} = \underline{\underline{\mathfrak{I}}} - \frac{1}{3}\underline{I}\,\underline{I} \qquad 3.5.2.14$$

Equations 3.5.2.9 - 14 now define $\frac{\partial r^{pl}}{\partial \underline{\varepsilon}}$ entirely in terms of quantities which are known.

The last term for the tangent operator can be derived simply by differentiating equation 3.4.1 with respect to temperature and is given by

$$\frac{\partial r^{pl}}{\partial \theta} = \frac{\eta}{2\Delta t}\Delta \bar{e}^{pl} Y \qquad 3.5.2.15$$

Chapter 4
THE FINITE ELEMENT MODEL

Finite element simulations were performed for two axisymmetric deep drawing cases. Both involved the drawing of a small axisymmetric cup from a circular blank but differed with respect to working conditions and dimensions. The first case was used to investigate certain aspects of the model - in particular, the effect of various material parameters and the effect of forming rate on the results: these results are discussed in Chapters 5 to 7. The second case was taken from a physical experiment for which the simulation results could provide interesting information: the results for this simulation are discussed in Chapter 8. The working conditions for both problems are given in Appendix A. The finite element model is similar in both cases and details are given below.

4.1 Geometry and Mesh

The finite element mesh used is shown in Figure 4.1. The sheet metal blank was discretised into two layers of 4-noded axisymmetric coupled temperature-displacement continuum elements with full integration. These elements were used so that changes in material properties (as a result of transformation induced plasticity) could be predicted through the thickness of the sheet. This follows from the discussion in Section 1.1.3. The choice of full integration was made to provide more accurate prediction of material property changes through the thickness of the blank. The blank material in the region of the punch contact was meshed coarsely since deformation in this area is limited by contact with the punch. The remainder of the blank material experiences large deformation, particularly the material drawn over the die radius, and hence is meshed more finely.

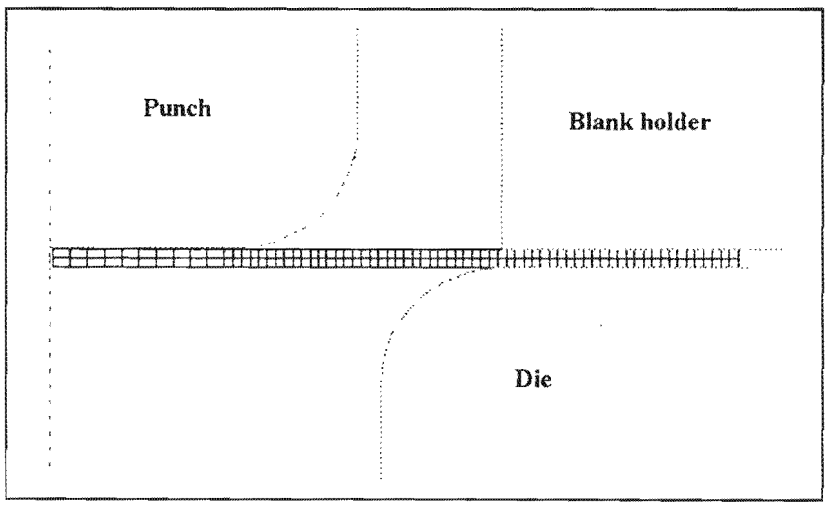

Figure 4.1 Finite Element Mesh

The tools (punch, die and blank holder) were modelled as perfectly rigid bodies using slideline elements in ABAQUS [12]. Suitable smoothing was employed in the region of punch and die radii to achieve the desired surfaces as shown in Figure 2.1.

The choice of slideline elements instead of rigid surfaces in ABAQUS was made due to the requirement of modelling heat effects in addition to friction at the tool/material interfaces. Nodes forming the slideline elements were tied using multi-point constraints so that the action of the tools could be applied easily by defining the motion of a single node in each tool.

4.2 Contact and Friction

Contact conditions were modelled using the interface elements combined with the slideline elements described above. 'Hard' contact pressure theory was used, i.e. no contact pressure exists until the surfaces are in contact at which point the contact pressure becomes infinite.

Friction was modelled using the classical Coulomb friction theory available with slideline interface elements in ABAQUS. The penalty method is used which allows small relative 'elastic slip' between surfaces which should be sticking. Friction coefficients were chosen to model the lubrication conditions at the tool/blank interfaces. The approximate values given below are those commonly used in the literature. The surface of the punch is, in practice, left unlubricated to avoid excessive thinning of the material over the punch radius - this interface is therefore given a high friction coefficient (about 0.25). The surfaces of the die and blank holder are usually lubricated to avoid excessive restraint of the blank which results in necking or tearing. These interfaces are therefore given lower coefficients of friction (about 0.1). This aspect of the model will be discussed further in Chapter 8.

4.3 Temperature Effects

Heat generation due to plastic work was included as a fraction of the plastic dissipation energy. This aspect is discussed in detail in Section 2.6.

Heat generation due to friction was also included in the model. ABAQUS models this frictional heat as a fraction of the total frictional energy dissipation. This fraction was assumed to be 0.8. Its effect on the results obtained is discussed further in Section 4 to determine the importance of the value chosen. It is also assumed that half of this frictional heat is conducted into each of the two contacting bodies.

Heat transfer to the tools was modelled via the conductance capability available with the interface elements used. The heat conducted to the tools is modelled by the following equation [12]:

$$q = k(\theta_a - \theta_b)$$

where q is the heat transferred, k is a factor called the gap conductance (a value of 5000 $W/m^2.K$ [17] was used in all simulations), and θ_a and θ_b are the temperatures of the two contacting surfaces.

Heat loss to the surrounding air from the exposed surfaces of the blank was neglected in the forming steps (see Section 4.4). The effect of this heat loss was assumed to be insignificant compared to heat loss to the tools.

The tools were assumed to remain at a constant temperature of 20°C. They have a large volume relative to the blank and were assumed to be heat sinks that are not heated to any significant degree by conduction from the deforming blank. The blank material was assumed to have an initial uniform temperature of 20°C. This is a reasonable approximation of the working conditions in a forming process.

4.4 Analysis Procedure

The finite element analysis of a typical forming problem was divided into four steps which constitute the simulation of the entire forming process. Most of the simulation results were, however, taken at the end of the second step - reasons for this will be discussed later.

1. The blank holder force was applied simulating the restraint of the metal blank. This force was applied as a ramp function over the time step.

2. The punch was moved through the intended displacement at the required speed (determined by the forming rate desired) while the holder force was kept constant. This step simulates the drawing process itself. The loading on the punch was applied as a 'ramp' function over the time step - this results in the punch having a constant velocity as desired in the analysis. This is not exactly the case in practice as in real forming processes the punch has a sinusoidal velocity.

3. The tools were removed while all the degrees of freedom of the formed blank were fixed. This step is included as a convenient means of setting the simulation up for the following step.

4. The boundary conditions on the formed component imposed in step 3 were relaxed to simulate elastic springback. This step excluded any heat effects since the process here involves no heat generation and is assumed to take place quickly enough to render heat loss due to convection negligible.

4.5 Forming Rate

The simulations reported in Chapter 6 were performed at different punch speeds to determine the effect of forming rate on the material variables of interest. The forming speed was applied by specifying different time lengths to the forming step (step 2 in Section 4.4 above). These different time lengths resulted in different constant velocities being imposed on the punch. The analyses were performed over time periods of 0.25, 2.5 and 25 seconds for a punch displacement of 25 mm resulting in punch speeds of 100, 10 and 1 mm/s.

4.6 Material Constants

The following material constants (Table 4.6) were used in all simulations. These are material parameters which were assumed to be independent of temperature and plastic strain.

Table 4.6 Material Constants for 304 Stainless Steel

Thermal Conductivity[1]	16.2 W/(mK)
Specific Heat[1]	502 J/(kgK)
Density[2]	7880 kg/m^3
Young's Modulus[2]	200 GPa
Poisson's Ratio[2]	0.29

[1] ref. 17
[2] ref. 19

Chapter 5
INVESTIGATION OF PARAMETERS

Certain parameters were used in the finite element simulations and the material model. The values of some of these parameters were estimated. It was therefore important to determine the sensitivity of the simulation results to changes in these parameters in order to evaluate the necessary accuracy in these estimates. The parameters of interest are:

1. Rate dependency parameters D and p
2. Frictional heat generation fraction

All other material constants and parameters used are assumed to be based on reliable experimental results in the sources quoted. The exception is friction coefficients. The values used for these were those commonly given in the literature for lubricated die and holder and an unlubricated punch and the effect of changes in these values will be discussed in Chapter 8. The simulations described in this Chapter were all performed on the same basic forming problem: the deep drawing of an axisymmetric cup; details of the working conditions can be found in Appendix A.1. The results illustrated are obtained at the end of Step 2 in the analysis procedure described in Section 4.4: this is at the end of the punch displacement before elastic springback - the reasons for this will be discussed in Chapter 7.

5.1 Rate Dependency Parameters

The parameters D and p in equation 2.3.1 determine the degree of rate dependency of the yield stress of the material. The values chosen for them should thus reflect the real behaviour of the material as far as possible. Since accurate values based on experimental work were not available for the material under investigation an estimate based on approximations using an existing rate dependency relation [17] as a guide was made. Figure 5.1 shows a comparison of the yield curve for 304 stainless steel obtained by using D = 50 and p = 2 in equation 2.3.1 and the yield curve given by Shinagawa *et al* [17]: both for a strain rate of 0.01/s. It was important to determine to what extent variations in these parameters affected material state variables of interest (particularly martensite content).

Simulations were performed for the following values of the parameters: D=40, p=3 and D=50, p=2; the first set of values representing greater strain rate dependence. The effect of changes in these parameters should be greatest for high rates of strain as can be deduced from equation 2.3.1. Test simulations were therefore conducted for a fast punch speed (100 mm/s) with the different values of D and p.

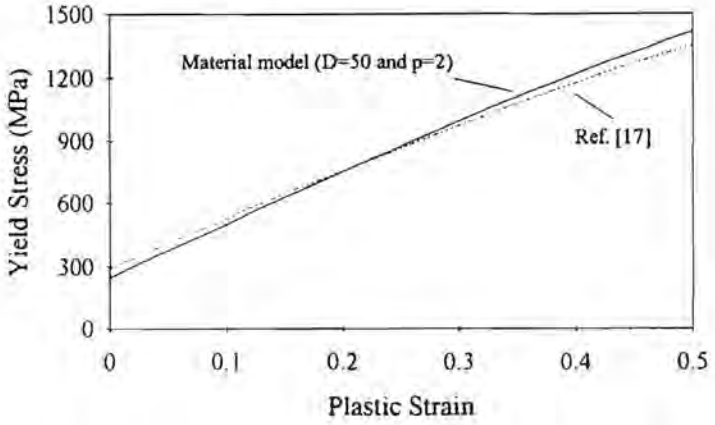

Figure 5.1 Yield stress of 304 stainless steel for $\dot{\bar{e}}^{pl} = 0.01/s$

5.1.1 Results

Plots showing the effect of these different values on the distribution of martensite and the yield stress are shown in Figures 5.1.1 and 5.1.2 respectively.

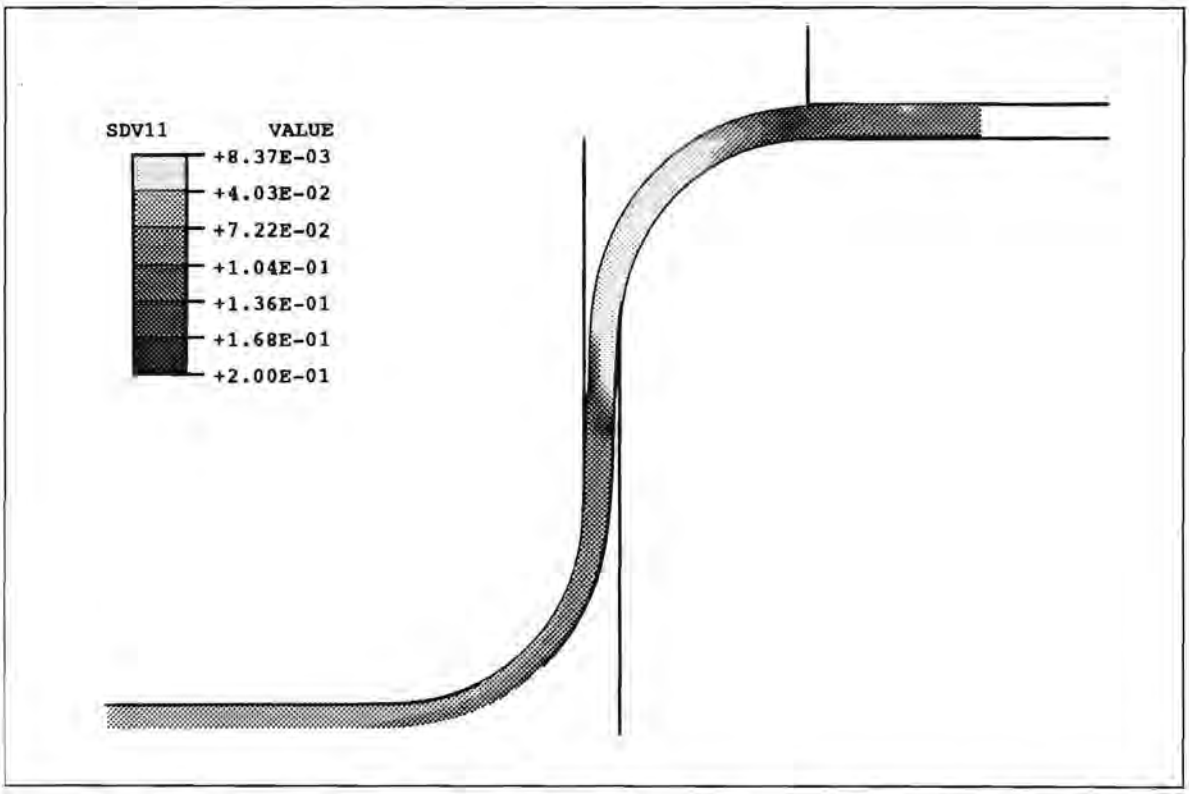

Figure 5.1.1-a Volume fraction of martensite: D = 50, p = 2

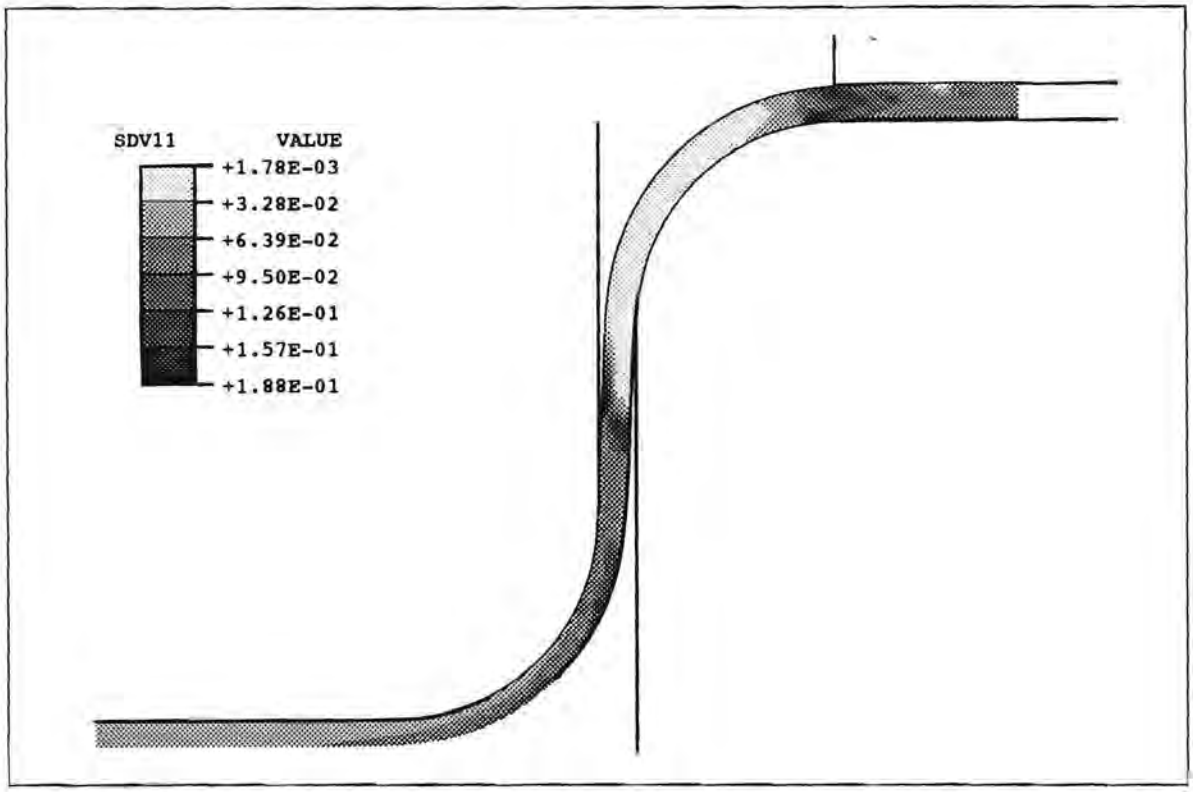

Figure 5.1.1-b Volume fraction of martensite: D = 40, p = 3

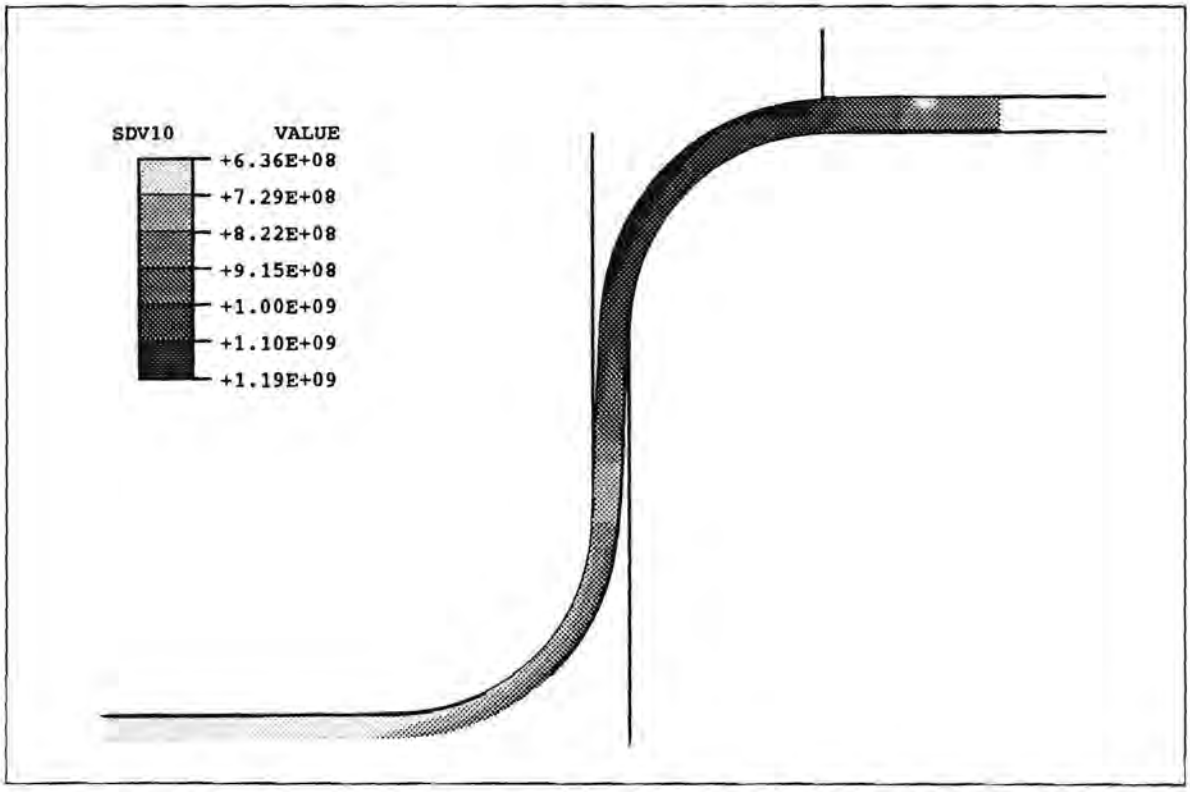

Figure 5.1.2-a Yield stress (Pa): D = 50, p = 2

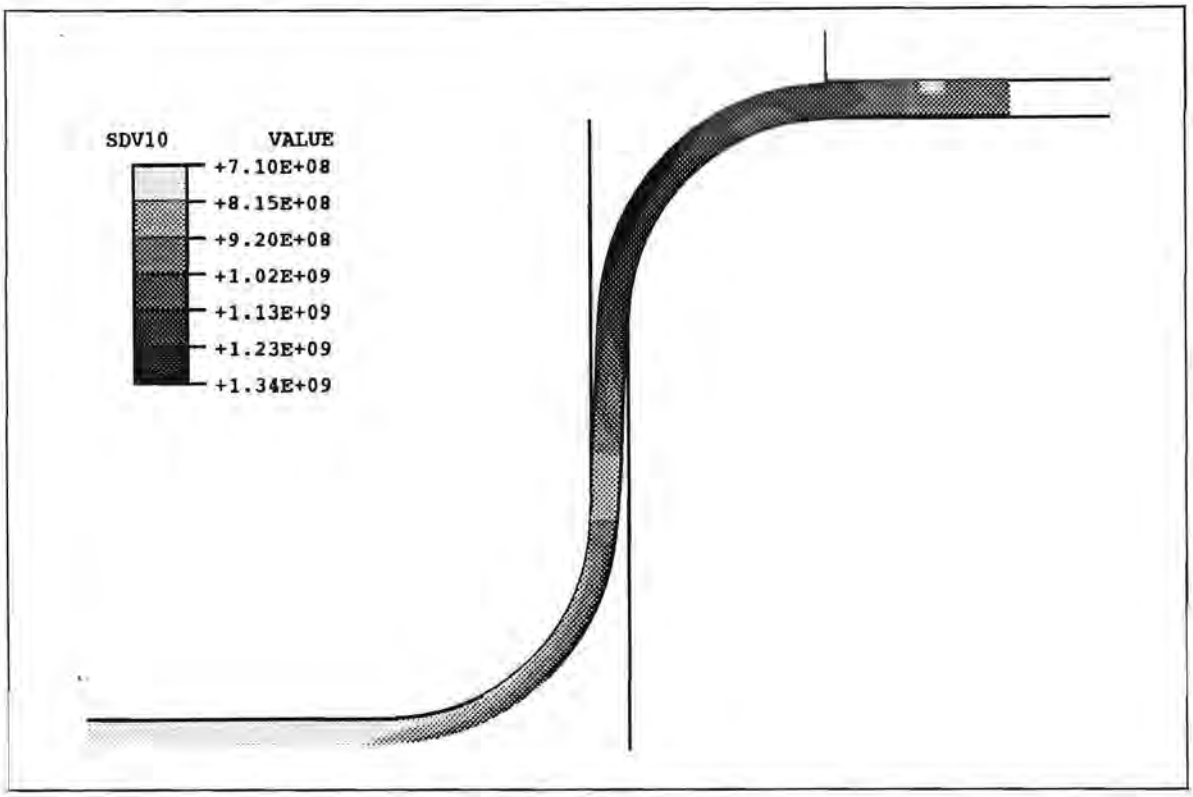

Figure 5.1.2-b Yield stress (Pa): D = 40, p = 3

5.1.2 Discussion

The results predicting the yield stress in the formed material show larger values for simulations using parameters representing greater strain rate dependence. This is expected when considering the effect of equation 2.3.1 on the value of the yield stress.

The results predicting the distribution of martensite show a lower level of martensite for greater strain rate dependence. This is caused by the higher yield stress resulting in greater plastic heat generation predicted by equation 3.4.1. This results in a higher working temperature for the deforming material and thus less tendency for martensite to form (Figure 2.1). The difference in the values is quite large in areas of low martensite content but in the areas of interest (i.e. high martensite content) the difference falls to below ten percent. The predicted distribution of martensite in both cases is, however, very similar.

These observations indicate that if accurate results are needed from which quantitative conclusions need to be drawn the values of D and p should be based on accurate experimental data. However, if all that is required from the simulation results is qualitative information regarding the distribution of martensite then the choice of these parameters is less critical.

Since the work covered in this study demands only qualitative comparisons it was decided that the values of these parameters could be chosen to suit the efficiency of the solution. The use of values of D and p representing greater strain rate dependence caused solution difficulties in certain cases. For this reason and on the basis of the comparison provided by Figure 5.1, it was decided that lower strain rate dependence would be used in all subsequent simulations (values of D=50 and p=2).

5.2 Frictional Heat Generation Fraction

In calculating the heat generated due to frictional energy dissipation the finite element code ABAQUS employs a fraction which approximates the amount of this dissipated energy converted to heat. Since most of the frictional dissipation energy is likely to be dissipated as heat this fraction was assumed to be quite large. Two test simulations comparing results for different values of this fraction were conducted with values of 0.8 and 0.7. The simulations were performed for a fast punch speed (100 mm/s) since for a fast forming rate heat effects have the greatest influence on the results: heat generated is given less time to conduct to the tools.

5.2.1 Results

Figure 5.1.1-a shows the predicted distribution of martensite in the formed component for a heat fraction of 0.8 and Figure 5.2.1 for a heat fraction of 0.7.

5.2.2 Discussion

The results for the larger heat generation fraction displayed in Figure 5.1.1-a show a lower level of martensite than that shown for the lower fraction in Figure 5.2.1. This is expected since greater heat generation will result in a higher working temperature for the deforming material and hence a lower tendency to form martensite (refer to Figure 2.1). However, the differences between the levels of martensite predicted by the two simulations are fairly small: of the order of less than five percent. This is far smaller than the difference in the actual values of the fractions used, which is greater than ten percent.

This indicates that the choice of an accurate value for this fraction is not critical. Since intuition suggests a fairly large value for this fraction a value of 0.8 was chosen to be used in all subsequent simulations.

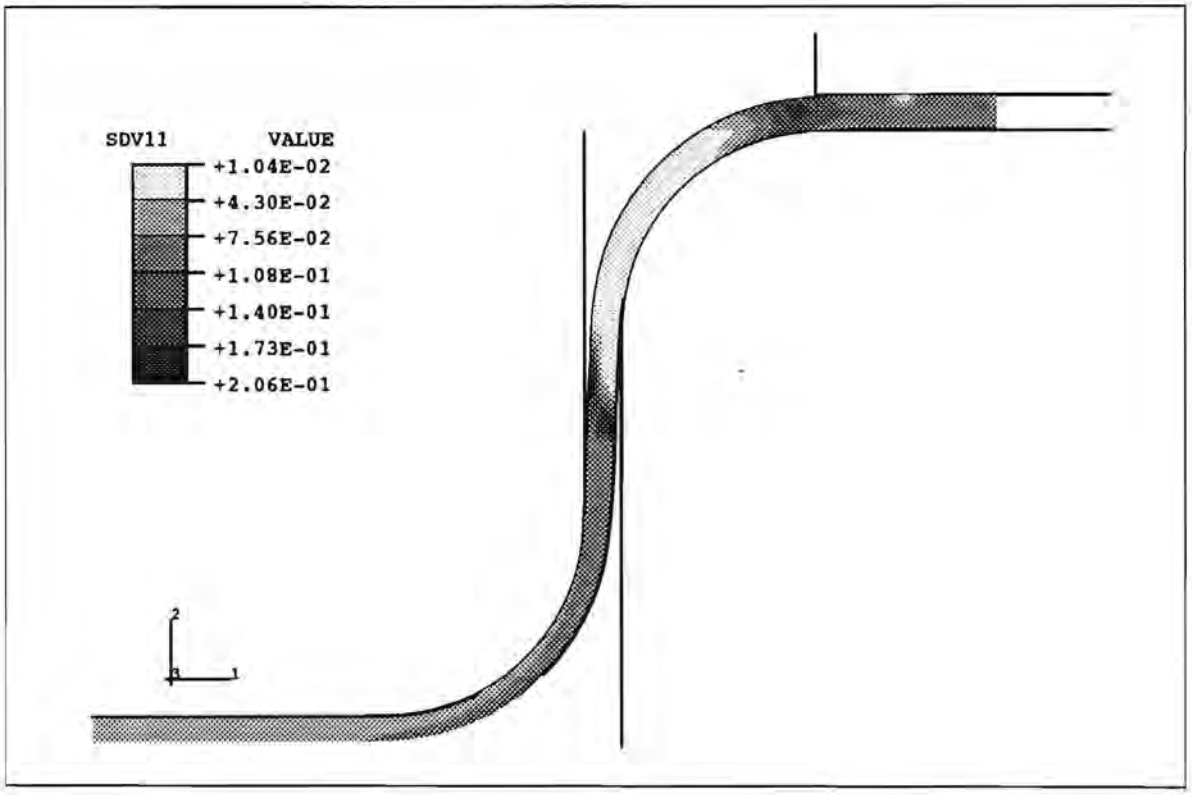

Figure 5.2.1 Volume fraction of martensite: heat generation fraction = 0.7

Chapter 6
THE EFFECT OF FORMING RATE

The previous chapter dealt with the effect of various parameters on the simulation results. This Chapter deals with the effect of forming rate on the predicted distribution of martensite in the formed component. The forming problem simulated here is the same as in Chapter 5: deep drawing of an axisymmetric cup (details of the working conditions are given in Appendix A.1). Forming rates determined by punch speeds of 100, 10 and 1 mm/s were investigated.

6.1 Results

The results shown were obtained at the end of forming Step 2 described in Section 4.4. Figures 6.1.1 show predicted distribution of martensite in the formed component for the three forming rates. Figures 6.1.2 and 6.1.3 show temperature and equivalent plastic strain distribution in the formed component for the fast forming rate.

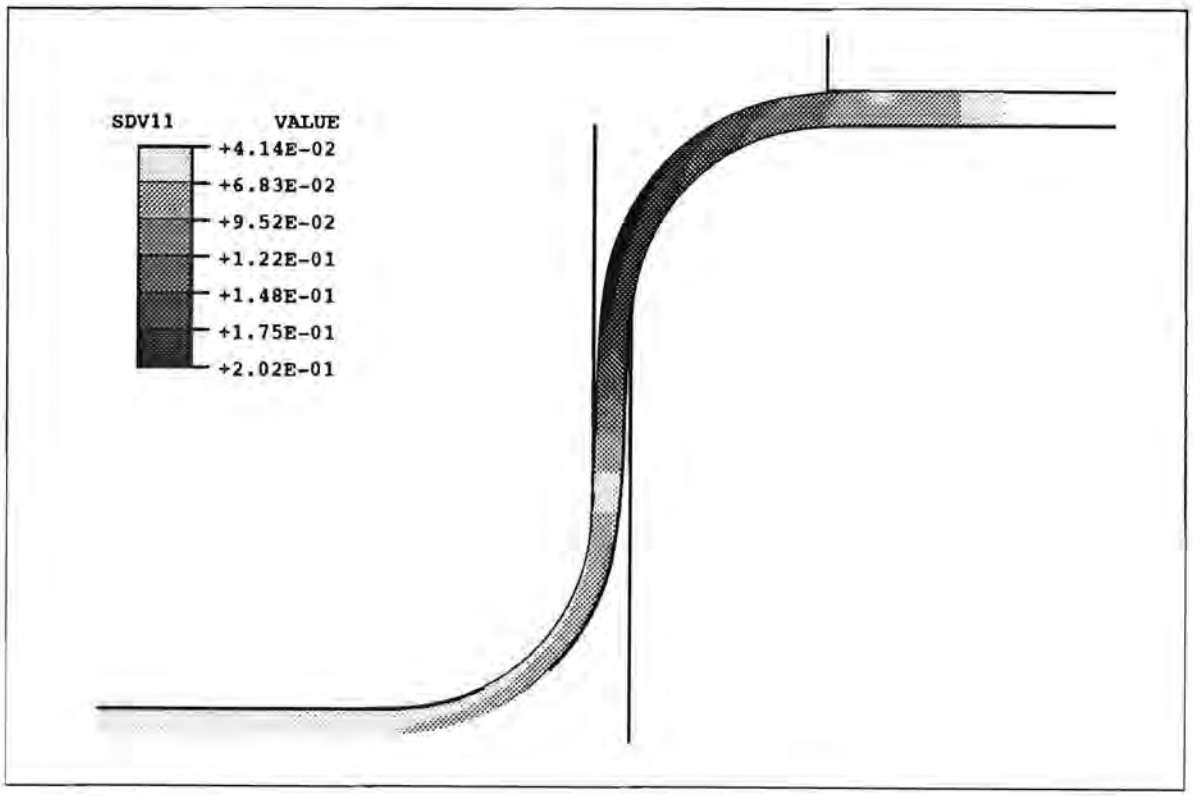

Figure 6.1.1-a Volume fraction of martensite: punch speed = 1 mm/s

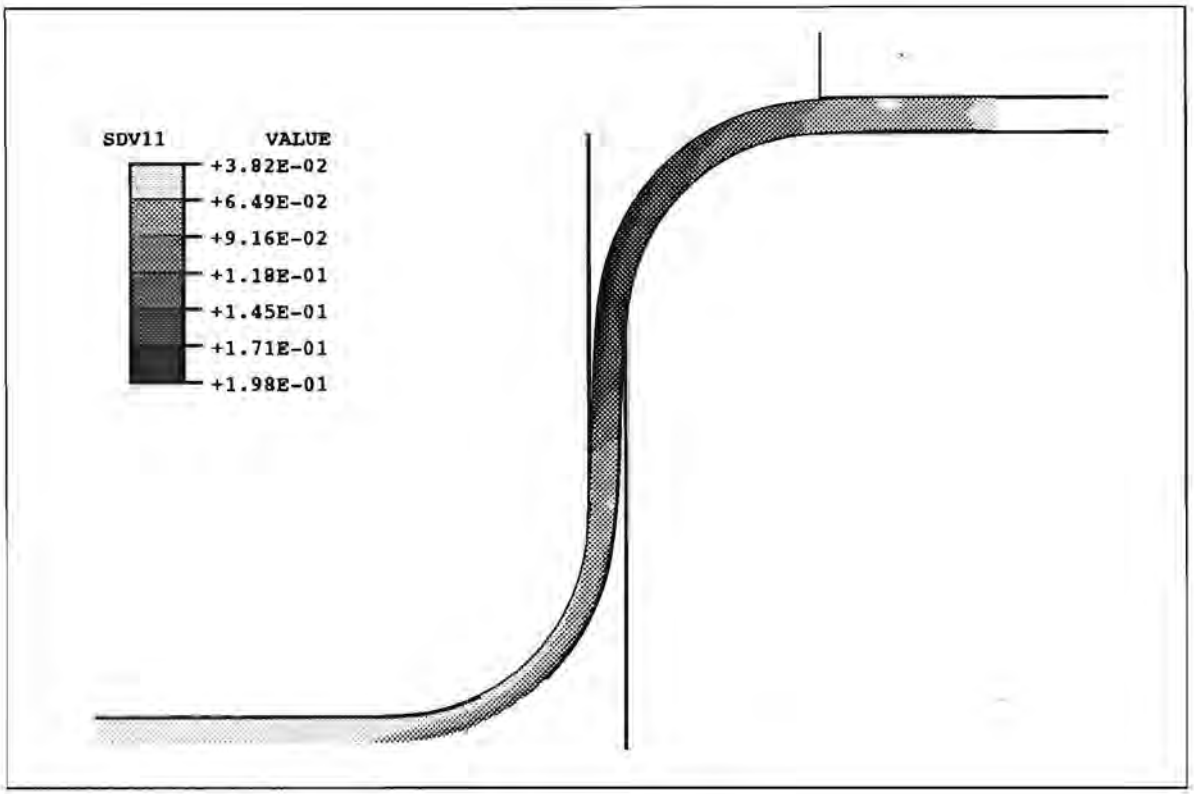

Figure 6.1.1-b Volume fraction of martesite: punch speed = 10 mm/s

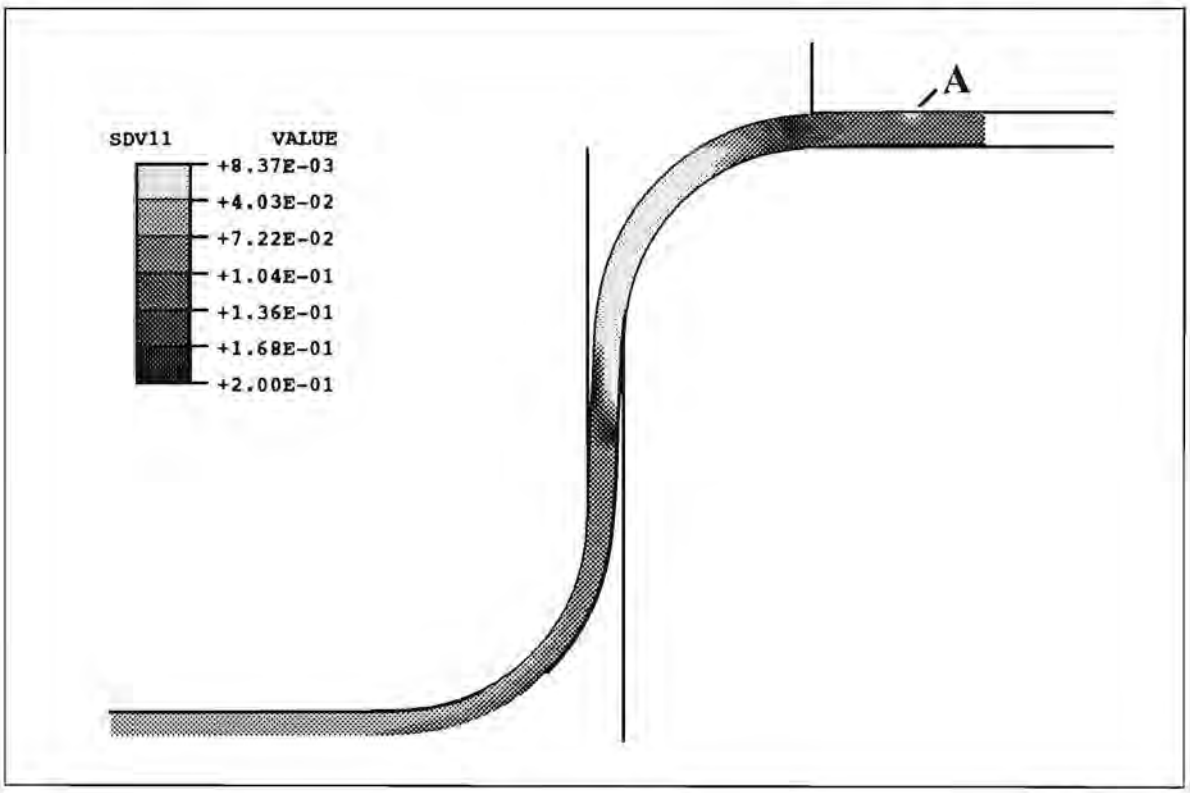

Figure 6.1.1-c Volume fraction of martensite: punch speed = 100 mm/s

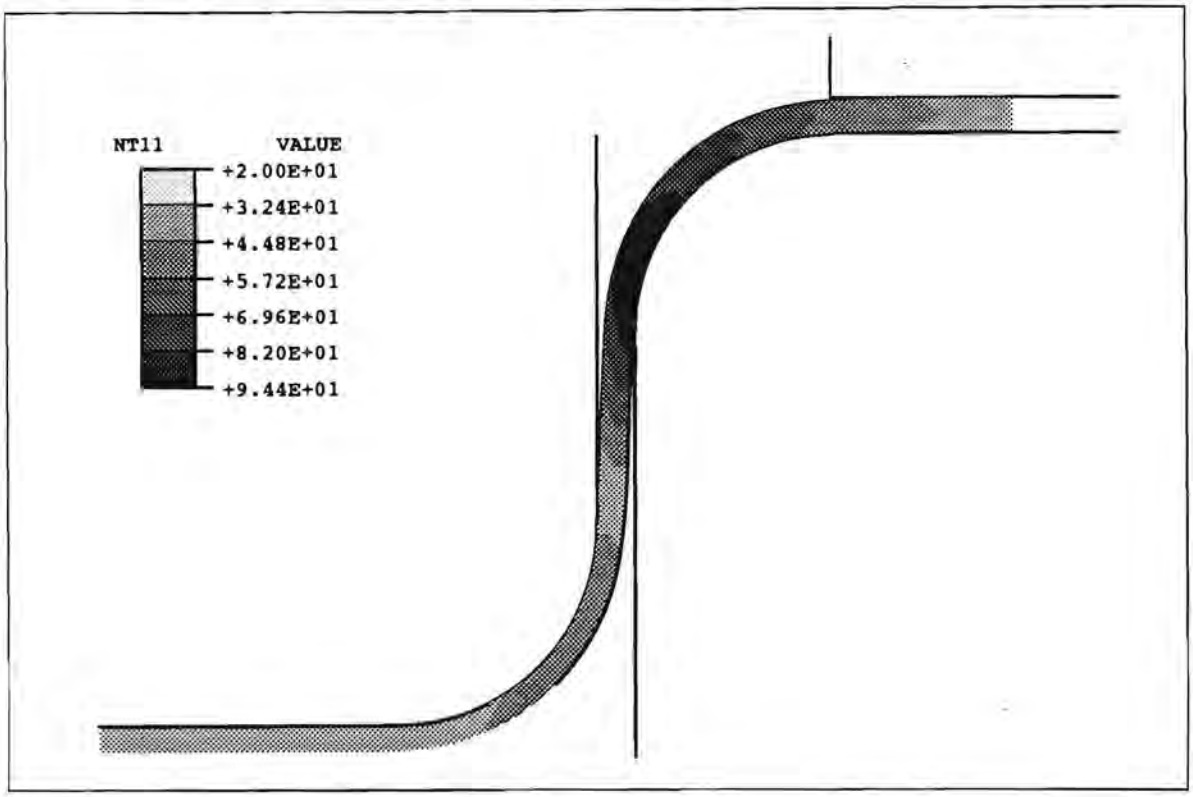

Figure 6.1.2 Temperature distribution: punch speed = 100 mm/s

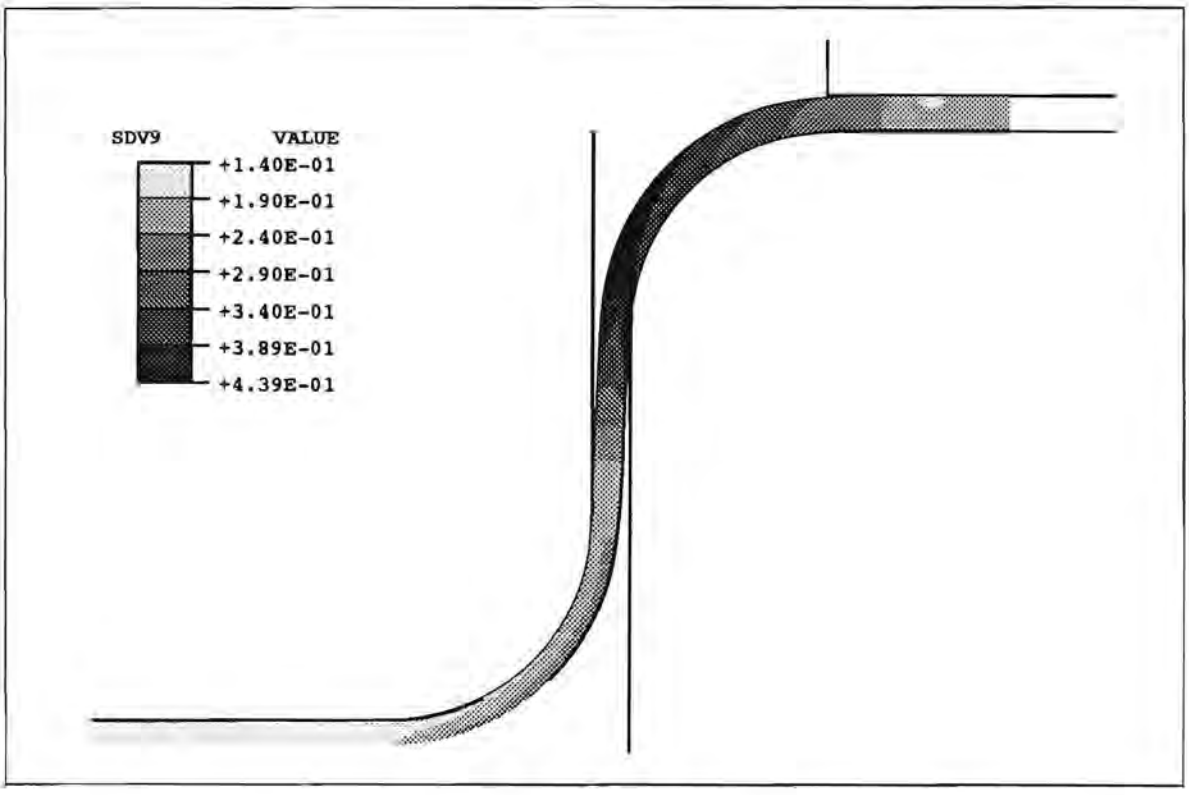

Figure 6.1.3 Equivalent plastic strain distribution: punch speed = 100 mm/s

6.2 Discussion

A comparison of the plots in Figures 6.1.1 reveals that the general level of martensite content is highest for the slow drawing rate but that it is most localised for the fast drawing rate. The intermediate drawing rate shows a distribution somewhere between these extremes.

These observations can be explained as follows:

1. Considering the problem independently of forming rate: the deforming material in the region of the die radius experiences both the highest frictional heating and the largest plastic straining.

2. For the slow drawing rate, heat generated by plastic work and friction has more time to conduct to the tools. Hence the working temperature of the blank is lower and the general level of martensite in the formed component is higher (refer to Figure 2), especially in the region of the die radius.

3. For the fast drawing rate heat generated has far less time to dissipate and consequently the overall level of martensite is lower - this is particularly evident in the region of the die radius where frictional heating is considerable (Figure 6.1.2). However, this also means that frictional heat does not have time to conduct to areas of the blank which do not experience frictional heating but still undergo large plastic straining (Figure 6.1.3). Consequently there are extremely localised areas of martensite concentration.

The points above describe the general trend observed that for a fast forming rate the formation of martensite is very localised and for a slow forming rate the level of martensite predicted is higher and its distribution throughout the blank is fairly even.

Chapter 7
SPRINGBACK AND COOLING

The results described in Chapters 5 and 6 were taken at the end of Step 2 in the finite element analysis procedure described in Section 4.4. The reasons for this are given by the results of the investigation described here. The same forming problem as described in the previous chapters is simulated here and the results at the end of Step 2 are compared with those after the springback and cooling simulations respectively.

7.1 Springback Analysis

Springback analyses were performed for two of the forming simulations described in the previous Chapter: for punch speeds of 1 and 100 mm/s. The springback is assumed to take place at a high rate so that any temperature changes are negligible. Both springback simulations were performed over a time period of 1 second.

Springback is essentially an elastic process but small amounts of plastic strain can occur due to high residual stresses. It should be noted that the purpose of these springback simulations was to investigate changes in martensite content and not the change in component shape as a result of the springback.

7.1.1 Results

The plots in Figures 7.2.1 and 7.2.2 show the predicted distribution of martensite in the formed component after springback for punch speeds of 1 mm/s and 100 mm/s.

7.1.2 Discussion

The plots in Figures 7.1.1 and 7.1.2 can be compared with those in Figures 6.1.1-a and 6.1.1-c which show predicted martensite distribution before springback. Both sets of plots show almost identical martensite distribution. However, small differences are evident:

1. The irregularity at point A in Figures 6.1.1 at the blankholder interface which is not evident in the springback plots is likely to be a numerical problem associated with the slideline forming the blankholder and has no physical meaning. The difference is, in any event, insignificant and can safely be ignored.

2. A slight difference is evident in Figure 7.1.1 at the centre of the cup. This is as a result of the imposition of an additional boundary condition here in this simulation which was necessary in order to obtain a converged solution: this can also be ignored.

3. There is a slight difference in the level of martensite content in certain areas. This is due to residual stresses being sufficiently large to cause small changes in plastic strain.

The above observations clearly show that springback has very little influence on the martensite distribution in the formed component. This is due to the fact that springback is predominantly an elastic process and elastic deformation has no influence on the martensite content of the material according to equation 2.5.1.

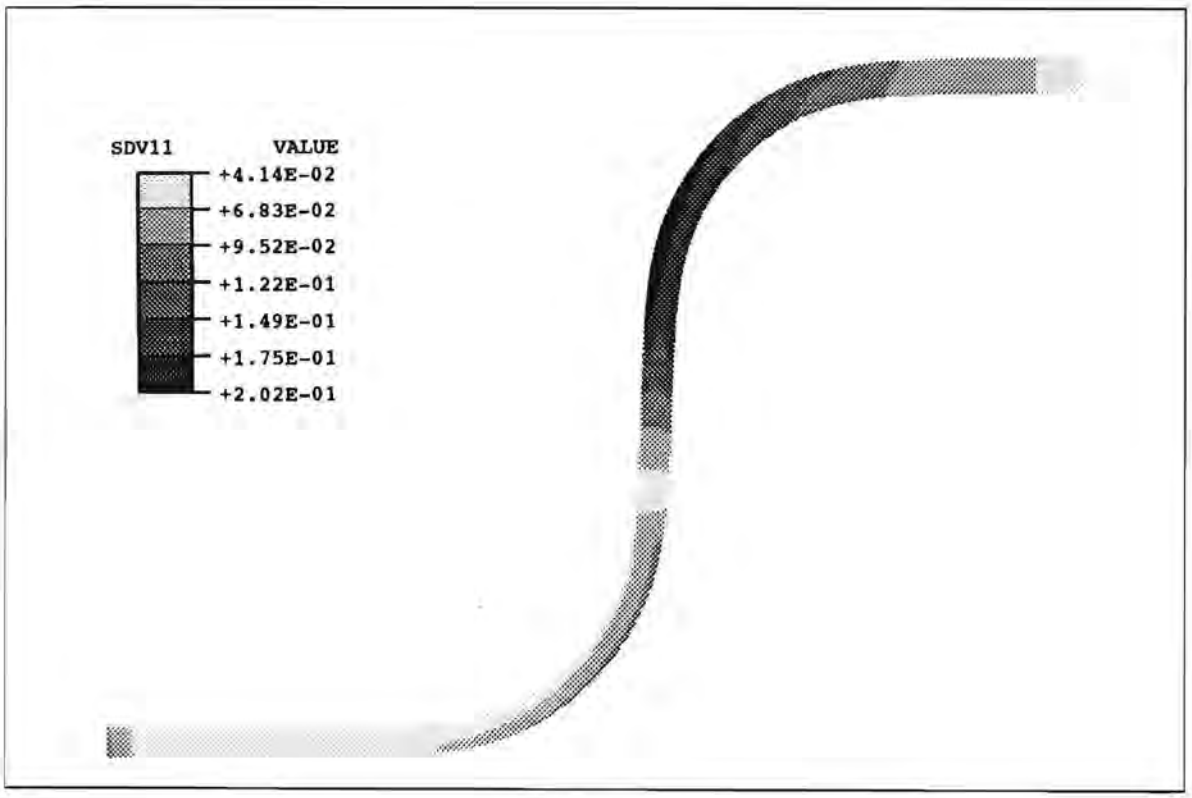

Figure 7.1.1 Volume fraction of martensite after springback: punch speed = 1 mm/s

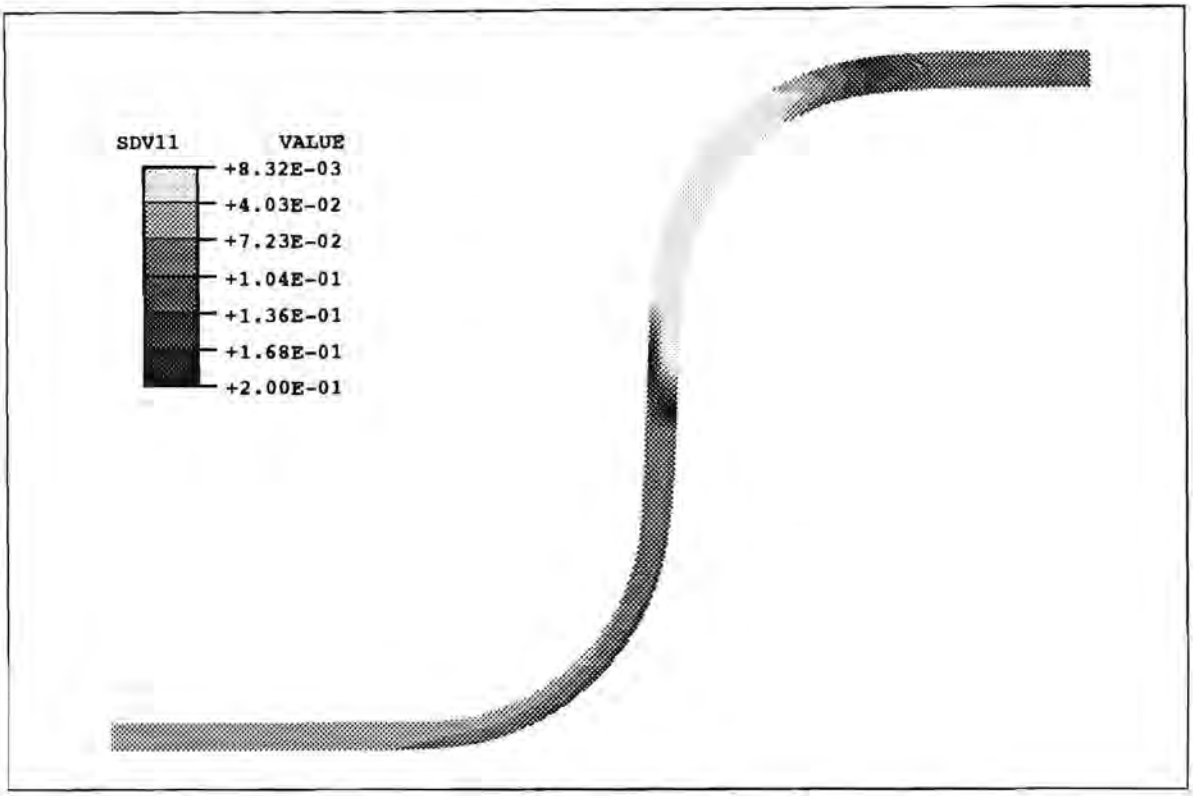

Figure 7.1.2 Volume fraction martensite after springback: punch speed = 100 mm/s

7.2 Cooling

The martensite evolution equation 2.5.1 predicts a change in martensite content in the material only for a change in plastic strain. Since thermal strains are neglected in the problem no strain would occur if the cooling of the formed component was simulated. Hence no change in martensite content would be predicted.

This means that with the finite element and material models used in this study, cooling of the formed component need not be simulated to get a complete prediction of martensite distribution.

Chapter 8
SIMULATION OF A DEEP DRAWING TEST

A series of deep drawing tests was performed by Sibanda and Knutsen [13] to investigate the formability of metastable austenitic stainless steels of different chemical compositions. The tests involved the same basic forming problem which was simulated using the finite element model described in Chapter 4 with the material model developed in this study. The purpose of this simulation was to obtain results predicting martensite distribution and equivalent plastic strain distribution in the formed component which could be compared with observations of the results of the forming tests. These observations concern the location of tearing in the failed specimens and the phenomenon of delayed cracking.

8.1 Description of the test and simulation

8.1.1 Geometry

The test involved the deep drawing of an axisymmetric cup of fixed dimensions from blanks of different diameters. For simplicity simulations were only performed for one blank diameter - 75 mm, which was the largest one used in the physical tests. The blank sheet thickness was 1 mm. The details of the dimensions and the working conditions of the set of tests are given in Appendix A.2.

8.1.2 Friction conditions

Since the entire surface of the blank was uniformly coated with a lubricant it was assumed that the punch and die/holder friction coefficients were approximately the same. To illustrate the effect of varying friction coefficients, and since the exact friction conditions of each test were not known, the simulation was repeated for different friction coefficients for the punch interface and a fixed coefficient for the die and holder interfaces.

8.1.3 Tearing and delayed cracking

The purpose of the drawing tests was to determine the formability of the steels hence each specimen was drawn until failure occurred. These failures were typically circumferential tearing at the locations indicated in Figure 8.1. With certain types of the steels tested in

reference [13] the phenomenon reported as delayed cracking occurred after failure of the material at A. This delayed cracking is visible as radial cracks which are regularly spaced around the circumference. They propagate towards the centre of the failed component over a period of hours after drawing. This phenomenon is not yet well understood and the information provided by a finite element simulation predicting the distribution of martensite in a typical test specimen could contribute to this understanding.

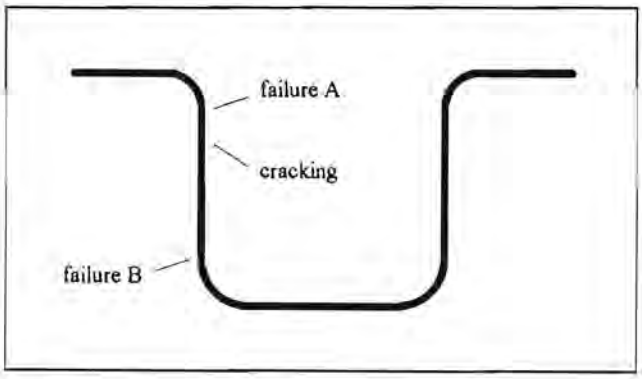

Figure 8.1 Location of failures in the test specimens

8.2 Results of the simulations

Simulations were performed with die and holder friction coefficients of 0.1 throughout and punch friction coefficients of 0.1 and 0.2. The plots showing distribution of martensite in the formed specimens are displayed in Figures 8.2.1. Plots showing the distribution of equivalent plastic strain are shown in Figures 8.2.2. It should be noted here that the material model developed in this study and used in these simulations does not predict failure of the material. These plots therefore show intact specimens which, in practice, may have failed at the level of deformation predicted.

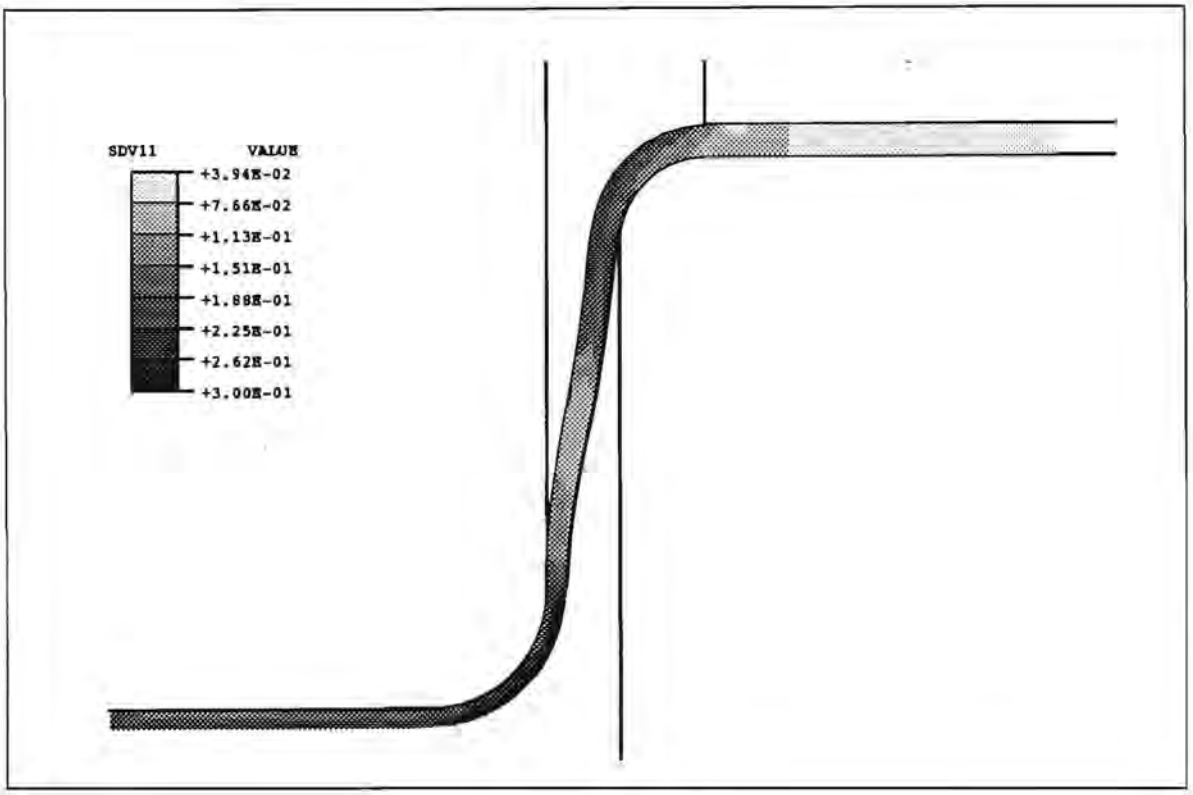

Figure 8.2.1-a Volume fraction of martensite in the test specimen: punch friction = 0.1

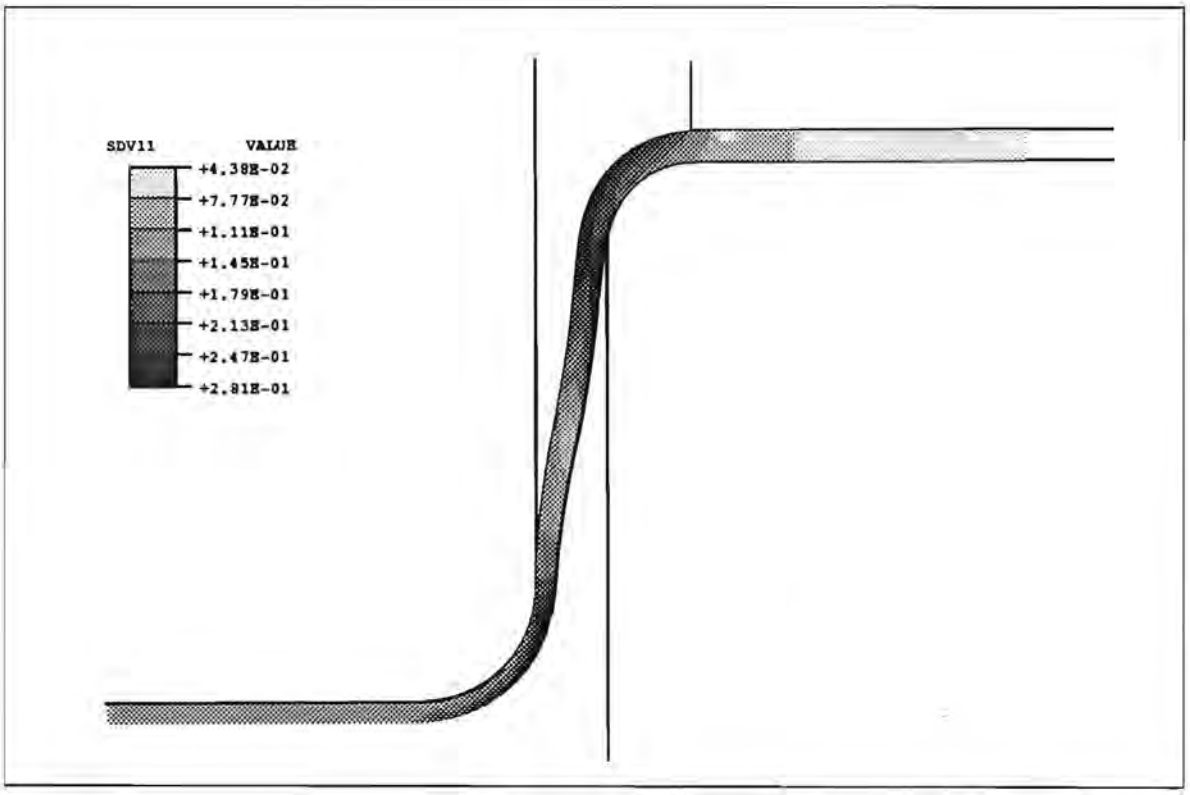

Figure 8.2.1-b Volume fraction of martensite in the test specimen: punch friction = 0.2

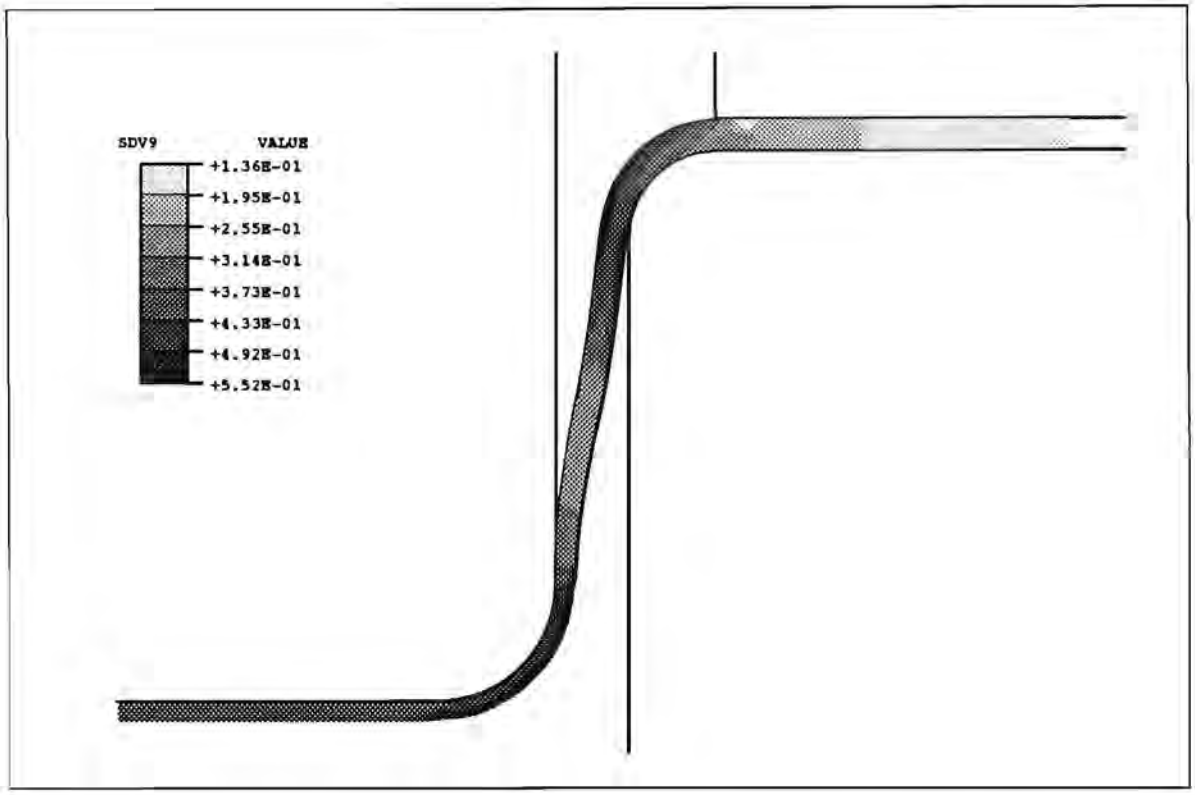

Figure 8.2.2-a Equivalent plastic strain in the test specimen: punch friction = 0.1

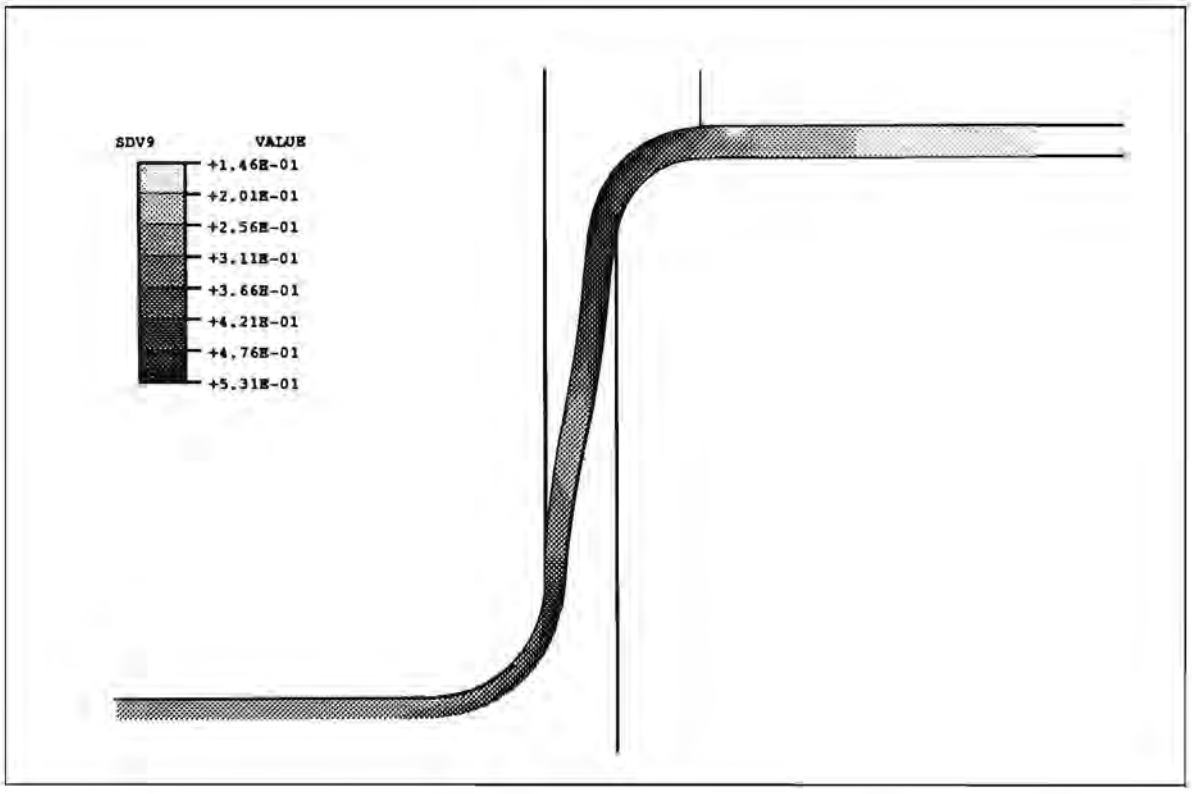

Figure 8.2.2-b Equivalent plastic strain in the test specimen: punch friction = 0.2

8.3 Discussion

The plots in Figures 8.2.1-a and 8.2.1-b show clearly two areas of interest - these correspond to the failure points marked in Figure 8.1. In these two areas there is a considerable concentration of high levels of martensite. An examination of the plots in Figures 8.2.2 shows that this is due to the large amount of plastic strain in these areas. The forming rate in this example is quite slow - hence the material temperature is not high enough to influence the martensite evolution to any extent. The reason that failure occurs in these areas is that, although the formation of martensite has a strengthening effect, the strain reaches sufficient levels to cause necking and ultimately tearing.

A comparison of the plots in Figures 8.2.1 reveals that for a higher punch friction coefficient the overall level of martensite is slightly higher but that this level is lower in the region of the punch corner. Figures 8.2.2 show that in the region of the punch corner there is far less plastic straining for a higher punch friction coefficient. This is because the increased friction of the punch prevents material from being stretched over its surface. This causes more material to be drawn in from the flange resulting in larger plastic strain at the die radius - this can be seen in Figure 8.2.2-b. What this implies is that for a low friction coefficient for the punch, failure is likely to occur at point B in Figure 8.1 but that for higher punch friction failure is likely to occur at point A. Failures in the test specimens occurred fairly randomly at either A or B thus it is quite likely that friction conditions at the punch interface varied for each test.

Finally, considering the phenomenon of delayed cracking, the distribution of martensite predicted in Figures 8.2.1 should be examined more closely. It can be seen that in the region of the die corner (the point from which cracks propagate after failure) the martensite distribution forms a gradient through the thickness of the material. A high level of martensite content occurs at the inner surface and a lower level at the outer surface. This is an important observation since martensite is less dense than austenite and the higher concentration in the inner surface may create stresses at the outer surface sufficient to induce cracking at this point.

Chapter 9
CONCLUSIONS AND RECOMMENDATIONS

The aim of this study was the development of a material model to predict the occurrence of transformation induced plasticity in metastable austenitic stainless steels and the influence this has on the properties of the steel. This model was to be applied in the finite element simulation of simple axisymmetric deep drawing examples.

The model was developed and implemented as the user material subroutine UMAT in ABAQUS. Finite element simulations were performed on two different axisymmetric deep drawing problems. The purpose of the simulations was firstly to investigate the effect of certain parameters on the results, secondly to investigate the effect of different forming rates, and finally to provide information which could explain certain phenomena observed in physical deep drawing tests.

The results obtained from the simulations predicted the distribution of plastic strain, yield stress, temperature and the volume fraction of martensite in the formed component. The predicted distribution of martensite can be used to explain certain observations in actual deep drawing tests.

9.1 Conclusions

From the results obtained the following conclusions can be drawn:

1. The material model developed here is successful in providing qualitative information on the distribution of martensite in a component formed by deep drawing. However, the model should not be used to provide accurate quantitative information on the amount of martensite present in a component formed by deep drawing.

2. From the limited comparison of simulation results with observations of a physical test the model seems to predict satisfactorily the enhanced plasticity properties of the material as a result of martensite formation.

3. The model can be used to help in the understanding of the phenomenon of delayed cracking in deep drawing test specimens.

9.2 Recommendations

Point 4 above introduces the following recommendation regarding future work in this study area. The predictions made by this material model are for a very broad range of stainless steel behaviour. Only certain chemical compositions of stainless steel exhibit delayed cracking, hence the following future research would be useful:

The material model developed here should be extended on the basis of experimental work to be conducted which would investigate the tendency of stainless steel of different compostions to undergo transformation induced plasticity. The extensions would serve to enable the model to be applied to specific stainless steels and provide accurate information of the behaviour of the material and its tendency to form martensite when plastically deformed. This would make possible more precise prediction of the occurrence of delayed cracking in certain materials.

References

1. Ameziane-Hassani, H and Neale, K W, 'On the analysis of sheet metal wrinkling', *Int. J. Mech. Sci.* **33**, 13 - 30 (1991).

2. Keeler, S P, 'Determination of forming limits in automotive stampings', *Sheet Metal Ind.* **42**, 683 - 691 (1965).

3. Chung, K and Shah, K, 'Finite element simulation of sheet metal forming for planar anisotropic materials', *Int. J. Plasticity*, submitted for publication.

4. Karafillis, A P and Boyce, M C, 'Tooling design in sheet metal forming using springback calculations', *Int. J. Mech. Sci.* **34**, 113 - 131 (1992).

5. Karafillis, A P, 'Tooling design for sheet metal forming using finite element analysis', MSc Thesis, MIT (1992).

6. Rebelo, N, Nagtegaal, J C, and Hibbitt, H D, 'Finite element analysis of sheet forming processes', *Int. J. Numer. Meth. Engng.* **30**, 1739 - 1758 (1990).

7. Nagtegaal, J C, and Rebelo, N, 'On the development of a general purpose finite element program for the analysis of forming processes', *Int. J. Numer. Meth. Engng.* **25**, 113 - 131 (1988).

8. Wang, N M, and Tang, S C, 'Analysis of bending effects in sheet forming processes', *Int. J. Numer. Meth. Engng.* **25**, 253 - 267 (1988).

9. Bellet, M, Massoni, E, and Chenot, J-L, 'Numerical simulation of thin sheet forming processes by the finite element method', *Eng. Comp.* 7, 21 - 31 (1990).

10. Yang, D Y, Shim, H B, and Chung, W J, 'Comparative investigation of sheet metal forming processes by elastic-plastic finite element method with emphasis on the effect of bending', *Eng. Comp.* 7, 274 - 281 (1990).

11. Peric, D and Owen, D R J, 'Computational model for 3-D contact problems with friction based on the penalty method', *Int. J. Numer. Meth. Engng.* **35**, 1289 - 1309 (1992).

12. *ABAQUS Version 5.2 Users', Theory and Example Problems Manuals*, Hibbitt, Karlsson and Sorensen Inc., Pawtucket, Rhode Island (1992).

13. Knutsen, R D and Sibanda, M, 'Evaluation of the formability of nitrogen alloyed metastable austenitic stainless steels', *Proc. Stainless Steel '93: Innovation Stainless Steel*, Florence (1993).

14. Ludwigson, D C and Berger, J A, 'Plastic behaviour of metastable austenitic stainless steels', *J. Iron Steel Inst.* **207**, 63-69 (1969).

15. Stringfellow, R G and Parks, D M, 'Rate dependent elastic-plastic behaviour of multiphase materials using ABAQUS', *Proc. ABAQUS Users' Conf.*, 497-513 (1990).

16. Stringfellow, R G, Parks, D M and Olson, G B, 'A constitutive model for transformation plasticity accompanying strain-induced martensite transformation in metastable austenitic steels', *Acta metall. mater.* **40**, 1703 - 1716 (1992).

17. Shinagawa, K, Mori, K and Osakada, K, 'Finite element simulation of deep drawing of stainless steel sheet with deformation-induced transformation', *J. Mater. Proc. Tech.* **27**, 301-310 (1991).

18. Mercer, C D, personal communication (1993).

19. Ledbetter, H M, 'Sound velocities and elastic constants steels 304, 310 and 316', *Met. Sci.* **14**, 595 - 596 (1980).

20. Barlat, F, Lege, D J, and Brem, J C, ' A six-component yield function for anisotropic materials', *Int. J. Plasticity* 7, 693 - 712 (1991).

21. Nakamachi, E, 'A finite element simulation of sheet metal forming processes', *Int. J. Numer. Meth. Engng.* **25**, 283 - 292 (1988).

22. Guo, Y Q, Batoz, J C, Detraux, J M, and Duroux, P, 'Finite element procedures for strain estimation of sheet metal formed parts', *Int. J. Numer. Meth. Engng.* **30**, 1385 - 1401 (1990).

23. Saran, M J, and Samuelsson, A, 'Elastic-viscoplastic implicit formulation for finite element simulation of complex sheet forming processes', *Int. J. Numer. Meth. Engng.* **30**, 1675 - 1697 (1990).

24. Germain, Y, Chung, K, and Wagoner, R H, 'A rigid-viscoplastic finite element program for sheet metal forming analysis', *Int. J. Mech. Sci.* **31**, 1 - 24 (1989).

25. Yang, D Y, Chung, W J, and Shim, H B, 'Rigid-plastic finite element analysis of sheet metal forming processes with initial guess generation', *Int. J. Mech. Sci.* **32**, 687 - 708 (1990).

26. Eterovic, A L, and Bathe, K-J, 'On the treatment of inequality constraints arising from contact conditions in finite element analysis', *Comp. Structures* **40**, 203 - 209 (1991).

27. Kumar, A and Singhal, L K, 'Effect of temperature and strain distribution on martensitic transformation during uniaxial testing of AISI-304 stainless steel', *Metall. Trans. A* **19A**, 1021-1026 (1988).

APPENDIX A

A.1 Working Conditions for Simulation 1

Punch diameter	40 mm
Die diameter	43 mm
Holder diameter	59 mm
Fillet radii	8 mm
Blank diameter	90 mm
Sheet thickness	1.2 mm
Holder force	4 kN
Punch displacement	25 mm
Punch speed	1 mm/s 10 mm/s 100 mm/s

A.2 Working Conditions for Simulation 2

Punch diameter	32 mm
Die diameter	35 mm
Holder diameter	41 mm
Fillet radii: Punch	4 mm
Die	3 mm
Blank diameter	75 mm
Sheet thickness	1 mm
Holder force	20 kN
Punch displacement	20 mm
Punch speed	1 mm/s

APPENDIX B

B.1 Derivation of terms $\frac{\partial \underline{\sigma}}{\partial \underline{\varepsilon}}$ and $\frac{\partial \underline{\sigma}}{\partial \theta}$ for the consistent modulus.

Variation of equation 3.3.7 in component form gives:

$$\left(1+\frac{3G}{q}\Delta\bar{e}^{pl}\right)\partial S_{ij}+\frac{3G}{q}S_{ij}\left(\partial\bar{e}^{pl}-\frac{\Delta\bar{e}^{pl}}{q}\partial q\right)=2G\partial\hat{e}_{ij} \qquad \text{B.1.1}$$

Variation of equation 3.3.3 using $\bar{\sigma}=q$ gives:

$$\partial q = H\partial\bar{e}^{pl}+Y\partial\theta \qquad \text{B.1.2}$$

Variation of equation 3.3.9 using $\bar{\sigma}=q$ gives:

$$\partial q+3G\partial\bar{e}^{pl}=2G\partial\bar{e} \qquad \text{B.1.3}$$

Substitution of B.1.2 into B.1.3 gives:

$$\partial\bar{e}^{pl}=\left(\frac{2G}{H+3G}\right)\partial\bar{e}-\left(\frac{Y}{H+3G}\right)\partial\theta \qquad \text{B.1.4}$$

Variation of equation 3.3.8 gives:

$$\partial\hat{e}_{ij}=\delta_{ik}\delta_{jl}\partial\varepsilon_{kl}-\frac{1}{3}\delta_{ij}\delta_{kl}\partial\varepsilon_{kl} \qquad \text{B.1.5}$$

Variation of equation 3.3.10 gives:

$$\partial\bar{e}=\frac{3}{2\bar{e}}\hat{e}_{ij}\partial\hat{e}_{ij} \qquad \text{B.1.6}$$

Substitution of equations B.1.2 - 7 into equation B.1.1 and simplifying gives:

$$\partial S_{ij}=\left[Q\left(\delta_{ik}\delta_{jl}-\frac{1}{3}\delta_{ij}\delta_{kl}\right)-RS_{ij}S_{kl}\right]\partial\varepsilon_{kl}+\frac{3GY}{q(H+3G)}S_{ij}\partial\theta \qquad \text{B.1.7}$$

Now, $$\partial\sigma_{ij}=\partial S_{ij}+K\delta_{ij}\delta_{kl}\partial\varepsilon_{kl} \qquad \text{B.1.8}$$

where K is the bulk modulus of the material. Substituting equation B.1.7 into B.1.8 gives:

$$\partial\sigma_{ij}=\left[Q\delta_{ik}\delta_{jl}+\left(K-\frac{1}{3}Q\right)\delta_{ij}\delta_{kl}-RS_{ij}S_{kl}\right]\partial\varepsilon_{kl}+\frac{3GY}{q(H+3G)}S_{ij}\partial\theta \qquad \text{B.1.9}$$

Where Q, R, H, Y, and G are defined in Section 3.5. Equation B.1.9 now completely defines the terms $\frac{\partial \underline{\sigma}}{\partial \underline{\varepsilon}}$ and $\frac{\partial \underline{\sigma}}{\partial \theta}$ in terms of known quantities.

B.2 Yield stress of austenitic phase given by Shinagawa et al [17]

$$\bar{\sigma}_a = 1788\bar{e} + B + 51.1\log\left(\frac{\dot{\bar{e}}}{0.001}\right) \qquad (\bar{e} < \bar{e}_c) \qquad \text{B.2.1}$$

$$\bar{\sigma}_a = B\left(\frac{\bar{e}_c - \bar{e}_i}{\bar{e} - \bar{e}_i}\right)^n + 1788\bar{e} + 51.1\log\left(\frac{\dot{\bar{e}}}{0.001}\right) \qquad (\bar{e} \geq \bar{e}_c) \qquad \text{B.2.2}$$

where $$n = 0.271\left(\frac{\dot{\bar{e}}}{0.001}\right)^{-0.068} \exp\left(\frac{234 + 107\log\left(\dot{\bar{e}} / 0.001\right)}{\theta + 273}\right)$$

$$B = 109\exp\left(\frac{226}{\theta + 273}\right)$$

$$\bar{e}_c = 0.0461\exp\left(\frac{302}{\theta + 273}\right)$$

$$\bar{e}_i = \bar{e}_c - n\frac{B}{182.3}$$

and $\bar{e}$ is the equivalent plastic strain.

B.3 Derivation of austenitic yield stress used in this study

The function for the austenitic yield stress used in this study is based on equations B.2.1 and B.2.2 with the following simplifications:

$$n = 0.6$$
$$B = 245 - 0.45\theta$$
$$\bar{e}_c = 0.129$$
$$\bar{e}_i = -0.65$$

These values are based on a strain rate of $\dot{\bar{e}} = 0.001$, to render equations B.2.1 and B.2.2 effectively rate independent, and a temperature of 20°C. The expression for B is replaced by the simple linear temperature dependence above. These changes give equations 2.4.2 and 2.4.3.

APPENDIX C

C.1 Listing of subroutine UMAT

```
c**********************************************************************
c
      subroutine UMAT(stress,statev,ddsdde,sse,spd,scd,
     1 rpl,ddsddt,drplde,drpldt,
     2 stran,dstran,time,dtime,temp,dtemp,predef,dpred,cmname,
     3 ndi,nshr,ntens,nstatv,props,nprops,coords,drot,pnewdt,
     4 celent)
c
      implicit real*8(a-h,o-z)
c
      character*8 cmname
      dimension stress(ntens),statev(nstatv),
     1 ddsdde(ntens,ntens),ddsddt(ntens),drplde(ntens),
     2 stran(ntens),dstran(ntens),time(2),predef(1),dpred(1),
     3 props(nprops),coords(3),drot(3,3),
     4 edev(4),sdev(4),dedev(4),enewd(4),enew(4),eplas(4),eelas(4),
     5 delast(4,4),spred(4),ehat(4),sprdev(4),plsdir(4),dplsdt(4),
     6 deplas(4),eeldev(4),eelt(4),s1(4),dspred(4),flodir(4)
c
c.....
c     User material definition - von Mises isotropic plasticity model
c     for 304 stainless steel - with transformation induced plasticity
c     Calculations performed for plane strain and axisymmetric cases.
c     Coded by: J D B Ward. July 1993.
c     Called by: ABAQUS.
c     Subroutines called: KINV,KPCURV,KETENS,KIJIJ,KMSTIF,KDEDE
c.....
c     Variables and constants not defined in ABAQUS user's manual:
c     blkmod  - bulk modulus
c     dedev   - increment of deviatoric strains
c     delast  - elastic constitutive tensor
c     depls   - increment of equivalent plastic strain
c     dsdep   - strain derivative of syield
c     dsdt    - temperature derivative of syield
c     dspred  - increment of elastic predictor stresses
c     epls    - equivalent plastic strain
c     dev  - first invariant (trace/3) of deviatoric strain increments
c     flodir  - plastic flow direction
c     phard   - slope of uniaxial hardening curve
c     pratio  - Poisson's ratio
c     s1      - stresses at start of increment
c     sprdev  - elastic predictor deviatoric stresses
c     spred   - elastic predictor stresses
c     sprdv   - trace/3 of elastic predictor stresses
c     sdev    - deviatoric stresses
c     syield  - value of current uniaxial yield stress
c     syist   - initial static yield stress
c     syird   - consistent initial rate dependent yield stress
c     shmod   - shear modulus
c     vfmart  - volume fraction of martensite
c     vfminp  - initial volume fraction of martensite
c     ymod    - Young's modulus
```

```
c.....
c
      zero = 0.0000D0
      one = 1.0D0
      two = 2.0D0
      three = 3.0D0
      twenty = 20.0D0
      r10m6 = 1.0D-6
      r10p6 = 1.0D6
c---  Inelastic heat fraction
      eta = 0.9000D0
c---  Young's Modulus and Poisson's Ratio for the material.
      ymod = props(1)
      pratio = props(2)
c---  Shear and Bulk moduli.
      shmod = ymod/(two*(one+pratio))
      blkmod = ymod/(three*(one-two*pratio))
c---  Rate dependency parameters
      dd = props(3)
      pp = props(4)
c
c---  Define the initial stress state and calculate
c---  deviatoric strain increment
      call KINV(dstran,dev)
      do 10 i = 1,ndi
       s1(i) = stress(i)
       dedev(i) = dstran(i) - dev
10    continue
      s1(4) = stress(4)
      dedev(4) = dstran(4)/two
c
c---  Calculate the elastic predictor stresses.
      call KETENS(delast,ymod,pratio,ndi,nshr,ntens)
      do 40 i = 1,ntens
       dspred(i) = zero
       do 40 j = 1,ntens
        dspred(i) = dspred(i) + delast(i,j)*dstran(j)
40    continue
      do 41 i = 1,ntens
       spred(i) = s1(i) + dspred(i)
41    continue
c
c---  Calculate deviatoric elastic predictor stresses
      call KINV(spred,sprdv)
      do 45 i = 1,ndi
       sprdev(i) = spred(i) - sprdv
45    continue
      sprdev(4) = spred(4)
c
c---  Estimate equivalent plastic strain rate
      call KIJIJ(dedev,depls1,ntens)
      depls1 = (6.000D-1)*depls1
      edot = depls1/dtime
c---  Obtain initial state quantities
      plsinp = statev(1)
      syinp = statev(2)
      vfminp = statev(3)
      syist = statev(5)
```

```
      teminp = temp + dtemp
c---  Calculate yield stress for input temp and strain rate.
      rdterm = ((edot/dd)**(one/pp) + one)
      sy0st = (245.0D0 - 4.5D-1*teminp)*r10p6
      sy0 = sy0st*rdterm
      syird = syist*rdterm
c---  Check for yield
      if(syird.gt.sy0) then
       ypoint = syird
      else
       ypoint = sy0
      end if
      call KIJIJ(sprdev,qelas,ntens)
      if(qelas.lt.ypoint) then
       sse = zero
       do 46 i = 1,ntens
        stress(i) = spred(i)
        do 46 j = 1,ntens
         ddsdde(i,j) = delast(i,j)
         ddsdde(j,i) = delast(j,i)
46     continue
       statev(1) = plsinp
       statev(2) = syinp
       statev(3) = vfminp
       statev(5) = syist
       goto 100
      end if
c
c---  Calc flow direction
      do 48 i = 1,ntens
       flodir(i) = three*sprdev(i)/(two*qelas)
48    continue
c
c---  Initial values for Newton loop
      depls = (qelas - sy0)/(three*shmod)
      epls = statev(5)
      vfminp = statev(11)
c
c---  Tolerances for Newton iterations
      numtry = 20
      dstres = r10m6*sy0
      tole = dstres/(three*shmod)
      tolf = dstres
c
c---  Newton method solution for depls
      do 20 i = 1,numtry
       plsinp = epls + depls
       call KPCURV(plsinp,depls,dtime,teminp,vfminp,
     1            syield,systat,dsdep,dsdt,vfmart,dd,pp)
       frhs = qelas - three*shmod*depls - syield
       dfdep = zero - three*shmod - dsdep
       cep = (zero - frhs)/dfdep
       depls = depls + cep
       if(dabs(cep).lt.tole.and.dabs(frhs).lt.tolf) goto 25
20    continue
      goto 100
25    continue
c
```

```
c--- Update equivalent plastic strain and yield stress.
     plsinp = epls + depls
     call KPCURV(plsinp,depls,dtime,teminp,vfminp,
     1          syield,systat,dsdep,dsdt,vfmart,dd,pp)
     epls = plsinp
c
c--- Calculate new deviatoric stresses.
     do 30 i = 1,ntens
       sdev(i) = two*syield*flodir(i)/three
30   continue
c
c--- Calculate true stress
     do 50 i = 1,ndi
       stress(i) = sdev(i) + sprdv
50   continue
     stress(4) = sdev(4)
c
c--- Update state variables.
     statev(1) = epls
     statev(2) = syield
     statev(3) = vfmart
     statev(4) = depls/dtime
     statev(5) = systat
c
c--- Calculate the material stiffness DDSDDE for the current increment.
     Q = two*shmod*syield/qelas
     B = dsdep/(three*shmod)
     R1 = two*shmod*three*(one-depls*dsdep/syield)
     R2 = two*syield*qelas*(one+B)
     R = R1/R2
     call KMSTIF(blkmod,Q,R,sdev,ddsdde,ntens)
c
c--- Calculate consistent initial yield stress
     rdterm = (depls/(dd*dtime))**(one/pp) + one
     syird = rdterm*syist
c
c--- Calculate heat generation rate.
     rpl = eta*depls*(syird + syield)/(two*dtime)
c
c--- Calc change strain derivative of rpl and temp derivative of stress.
     call KDEDE(depls,flodir,sdev,syist,syield,ddsdde,
     1          dsdep,dsdt,shmod,dtime,drplde,ddsddt,dd,pp)
c
c--- Calculate temp derivative of rpl
     drpldt = eta*depls*dsdt/(two*dtime)
c
100  continue
c
     return
     end
c
c**********************************************************************
c
     subroutine KINV(tensor,tinv1)
c.....
c    Routine to calculate the first invariant of a tensor.
c    Called by UMAT.
c.....
```

```
c
      implicit real*8(a-h,o-z)
c
      dimension tensor(4)
c
      zero = 0.000D0
      one = 1.0D0
      two = 2.0D0
      three = 3.0D0
c
c---  Calculate first invariant of tensor.
      trace = zero
      do 10 i = 1,3
       trace = trace + tensor(i)
10    continue
      tinv1 = trace/three
c
      return
      end
c
c**********************************************************************
c
      subroutine KPCURV(plsinp,depls,dtime,teminp,vfminp,
     1                  syield,systat,dsdep,dsdt,vfmart,dd,pp)
c.....
c     Routine containing the plasticity curve
c     Returns the yield stress and its derivatives for a given
c     plastic strain, time increment and temperature.
c     Called by UMAT.
c.....
c
      implicit real*8(a-h,o-z)
c
      zero = 0.00000D0
      one = 1.000000D0
      two = 2.000D0
      r10p6 = 1.000D6
c
c---  Find value of static yield stress for austenite phase and its derivatives
      tabs = teminp + 273.0D0
      ecrit = 0.1290D0
      bb = 245.0D0 - 4.50D-1*teminp
      edot = depls/dtime
      tnn = 0.600D0
      ei = zero - 0.650D0
      eh = (ecrit-ei)/(plsinp-ei)
c
      dehde = (ei - ecrit)/((plsinp-ei)**two)
c
      if(plsinp.lt.ecrit) then
       syaust = (1788.0D0*plsinp+bb)*r10p6
       dsade = 1788.0D0*r10p6
       dsadt = -4.500D-1*r10p6
      else
       syaust = (bb*eh**tnn + 1788.0D0*plsinp)*r10p6
       dsade = (1788.0D0 + bb*tnn*eh**(tnn-one)*dehde)*r10p6
       dsadt = -4.500D-1*eh**tnn*r10p6
      end if
```

```
c
c--- Find volume fraction and strain and temp derivatives
c    of martensite.
     call KVMART(plsinp,teminp,vfminp,vfmart,dvmdep,depls,
    1            dvmdt)
c
c--- Calculate combined yield stress
     symart = 1591.00D6
     Q = 0.8500D0
     qm1 = Q - one
     vfaust = one - vfmart
     systat = syaust*vfaust + symart*vfmart**Q
c
c--- Strain and temp derivatives of yield stress
     dsstde = vfaust*dsade + dvmdep*(Q*symart*vfmart**qm1 - syaust)
     dsstdt = dsadt*vfaust + (Q*symart*vfmart**qm1-syaust)*dvmdt
c
c--- Calculate rate dependent terms
     term1 = (edot/dd)**(one/pp) + one
     term2 = ((edot/dd)**(one/pp))/(pp*depls)
     syield = systat*term1
     dsdep = dsstde*term1 + systat*term2
     dsdt = dsstdt*term1
c
     return
     end
c
c*************************************************************************
c
     subroutine KVMART(plsinp,teminp,vfminp,vfmart,dvmdep,depls,
    1                  dvmdt)
c.....
c    Routine contains the volume fraction-temperature relations
c    for the martensite phase.
c    Returns the vol fraction of martensite for a given temp,
c    strain and input vol fraction.
c    Called by KPCURV.
c.....
c
     implicit real*8(a-h,o-z)
c
     dimension datkk(7),datff(7),datss(7),datt(7)
c
c--- Data for temperature dependent parameters.
     data datkk/0.0D0,6.5D0,11.0D0,17.0D0,31.0D0,1006.0D0,2626.0D0/
     data datss/1.0D0,0.055D0,0.02D0,0.003D0,0.0001D0,0.0D0,0.0D0/
     data datff/1.0D0,0.64D0,0.46D0,0.33D0,0.22D0,0.03D0,0.0D0/
     data datt/0.0D0,20.0D0,30.0D0,40.0D0,50.0D0,70.0D0,100.0D0/
c
     one = 1.000D0
     two = 2.000D0
     six = 6.000D0
c
c--- Find values of parameters k,f and s for input temperature.
     do 10 i = 1,7
      if(teminp.lt.datt(i)) then
        k = i
        goto 20
```

```
      end if
      k = i
10    continue
c---  Interpolate value linearly from data
20    continue
      if (k.eq.1) then
       pkk = datkk(1)
       pss = datss(1)
       pff = datff(1)
       dkkdt = (datkk(2)-datkk(1))/(datt(2)-datt(1))
       dssdt = (datss(2)-datss(1))/(datt(2)-datt(1))
       dffdt = (datff(2)-datff(1))/(datt(2)-datt(1))
      else
       factor = (datt(k) - teminp)/(datt(k)-datt(k-1))
       diff = datkk(k) - datkk(k-1)
       pkk = datkk(k) - diff*factor
       dkkdt = (datkk(k)-datkk(k-1))/(datt(k)-datt(k-1))
       diff = datss(k) - datss(k-1)
       pss = datss(k) - diff*factor
       dssdt = (datss(k)-datss(k-1))/(datt(k)-datt(k-1))
       diff = datff(k) - datff(k-1)
       pff = datff(k) - diff*factor
       dffdt = (datff(k)-datff(k-1))/(datt(k)-datt(k-1))
      end if
c
c---  Calc volume fraction of martensite by backward Euler.
      vfmart = vfminp + pkk*(vfminp + pss)*(pff - vfminp)*depls
c---  Calc strain and temp derivatives of vfmart
      dvmdep = pkk*(vfmart + pss)*(pff - vfmart)
      term1 = vfminp**two + (pff-pss)*vfminp - pff*pss
      term2 = (dffdt-dssdt)*vfminp - (dffdt*pss+dssdt*pff)
      dvmdt = (dkkdt*term1 + pkk*term2)*depls
c
      return
      end
c
c**********************************************************************
c
      subroutine KETENS(delast,ymod,pratio,ndi,nshr,ntens)
c.....
c     Routine to define the elastic constitutive tensor.
c     Called by UMAT.
c.....
c
      implicit real*8(a-h,o-z)
c
      dimension delast(ntens,ntens)
c
      zero = 0.000D0
      one = 1.0D0
      two = 2.0D0
      three = 3.0D0
      coeff = ymod/((one+pratio)*(one-two*pratio))
c
c---  Values of elastic constitutive tensor delast.
      delast(1,1) = coeff*(one-pratio)
      delast(1,2) = coeff*pratio
      delast(1,3) = coeff*pratio
```

```
      delast(1,4) = zero
      delast(2,1) = coeff*pratio
      delast(2,2) = coeff*(one-pratio)
      delast(2,3) = coeff*pratio
      delast(2,4) = zero
      delast(3,1) = coeff*pratio
      delast(3,2) = coeff*pratio
      delast(3,3) = coeff*(one-pratio)
      delast(3,4) = zero
      delast(4,1) = zero
      delast(4,2) = zero
      delast(4,3) = zero
      delast(4,4) = coeff*(one-two*pratio)/two
c
      return
      end
c
c**********************************************************************
c
      subroutine KIJIJ(tensor,svar,ntens)
c.....
c     Routine to calculate the quantity sqrt(3/2*tij*tij) of a tensor.
c     Called by UMAT.
c.....
c
      implicit real*8(a-h,o-z)
c
      dimension tensor(ntens)
c
      one = 1.0D0
      two = 2.0D0
      three = 3.0D0
c
      var1 = tensor(1)**2 + tensor(2)**2 + tensor(3)**2
      var2 = two*tensor(4)**2
      var = three*(var1 + var2)/two
      svar = sqrt(var)
c
      return
      end
c
c**********************************************************************
c
      subroutine KMSTIF(bk,q,r,devsts,ddsdde,ntens)
c.....
c     Routine to calculate derivative of stress tensor with respect to strain
c     Called by UMAT.
c.....
c
      implicit real*8(a-h,o-z)
c
      dimension devsts(ntens),ddsdde(ntens,ntens)
c
      one = 1.0D0
      two = 2.0D0
      three = 3.0D0
c
      ddsdde(1,1) = bk + two*q/three - r*devsts(1)**2
```

```
      ddsdde(2,2) = bk + two*q/three - r*devsts(2)**2
      ddsdde(3,3) = bk + two*q/three - r*devsts(3)**2
      ddsdde(1,2) = bk - q/three - r*devsts(1)*devsts(2)
      ddsdde(1,3) = bk - q/three - r*devsts(1)*devsts(3)
      ddsdde(2,3) = bk - q/three - r*devsts(2)*devsts(3)
      ddsdde(4,4) = q/two - r*devsts(4)**2
      ddsdde(1,4) = -r*devsts(1)*devsts(4)
      ddsdde(2,4) = -r*devsts(2)*devsts(4)
      ddsdde(3,4) = -r*devsts(3)*devsts(4)
      do 10 i = 1,ntens
        do 10 j = 1,ntens
          ddsdde(j,i) = ddsdde(i,j)
10    continue
c
      return
      end
c
c**********************************************************************
c
      subroutine KDEDE(depls,en,sd,si,sy,dsde,dh,dth,gg,dt,
     1                 drde,dsdt,dd,pp)
c.....
c     Routine to calc strain derivative of heat generation (rpl)
c     and temperature derivative of stress.
c     Called by UMAT.
c.....
c
      implicit real*8(a-h,o-z)
c
      dimension en(4),dsde(4,4),drde(4),sd(4),dep(4),dede(4),dsdt(4)
c
      zero = 0.000D0
      one = 1.000D0
      two = 2.000D0
      three = 3.000D0
      t23 = two/three
      t13 = one/three
      eta = 0.9000D0
c
c---  Calc derivative of plastic strain wrt total strains
      do 20 i = 1,4
       dede(i) = en(1)*(t23*dsde(1,i)-t13*(dsde(2,i)+dsde(3,i)))/dh+
     1           en(2)*(t23*dsde(2,i)-t13*(dsde(1,i)+dsde(3,i)))/dh+
     2           en(3)*(t23*dsde(3,i)-t13*(dsde(2,i)+dsde(1,i)))/dh+
     3  two*en(4)*dsde(4,i)/dh
20    continue
c
c---  Derivative of rpl wrt total strains
      sird = si*((depls/(dt*dd))**(one/pp) + one)
      do 30 i = 1,4
        drde(i) = eta*dede(i)*(sird + sy + depls*dh
     1     + si*((depls/(dd*dt))**(one/pp))/pp)/(two*dt)
30    continue
c
c---  Temperature derivative of stress
      do 50 i = 1,4
       dsdt(i) = three*gg*dth*sd(i)/(sy*(dh + three*gg))
50    continue
```

```
c
      return
      end
c
c*************************************************************************
```

C.2 Input deck for a typical simulation

```
*HEADING,UNSYMM
DEEP DRAWING OF A CYLINDRICAL CUP
** Axisymmetric drawing of a stainless steel cup
** Coupled temperature-displacement analysis
** Drawing speed = 100 mm/s
** J D B Ward, July 1993
*RESTART,WRITE,FREQ=50
**DATA CHECK
**
** Define nodes
*NODE
** Blank
101,0.,0.
181,0.045,0.
201,0.0,0.0006
281,0.045,0.0006
301,0.0,0.0012
381,0.045,0.0012
** Punch
600,0.012,0.0093
601,-0.0001,0.001299
602,0.012,0.0013
612,0.02,0.0093
613,0.02,0.025
** Die
500,0.0295,-0.0080
501,0.0215,-0.025
502,0.0215,-0.0080
512,0.0295,0.0000
513,0.048,0.0000
** Holder
401,0.0295,0.025
402,0.0295,0.00121
403,0.02951,0.0012
404,0.048,0.0012
5000,0.045,-0.025
4000,0.045,0.025
6000,0.,0.025
**
** Generate Nodes
** Blank
*NGEN,NSET=BOT
101,181,1
*NGEN,NSET=TOP
```

```
301,381,1
*NGEN,NSET=MID
201,281,1
*NSET,NSET=WRKPC
BOT,TOP
** Die
*NGEN,NSET=D1,LINE=C
502,512,1,500
*NSET,NSET=D2
513
*NSET,NSET=DIE1
D1,D2
** Punch
*NGEN,NSET=P1,LINE=C
602,612,1,600
*NSET,NSET=P2
613
*NSET,NSET=PUNCH1
P1,P2
** Holder
*NSET,NSET=HOLDER1
401,402,403,404
*NSET,NSET=DIE
501
*NSET,NSET=PUNCH
601
*NSET,NSET=HOLDER
403
*NSET,NSET=TOOLS
PUNCH,DIE,HOLDER
*NSET,NSET=TOOLS1
DIE1,PUNCH1,HOLDER1
*NSET,NSET=CENTER
101,201,301
*NSET,NSET=BLANK
BOT,TOP,MID
**
** Blank Elements
*ELEMENT,TYPE=CAX4T
101,101,103,203,201
*ELGEN,ELSET=B1
101,10,2,1,2,100,100
*ELEMENT,TYPE=CAX4T
111,121,122,222,221
*ELGEN,ELSET=B2
111,60,1,1,2,100,100
*ELSET,ELSET=BLANK
B1,B2
*ELSET,ELSET=TOP,GENERATE
201,270,1
*ELSET,ELSET=BOT,GENERATE
101,170,1
**
** Interface elements
*ELEMENT,TYPE=ISL21AT
401,341,342
*ELGEN,ELSET=HOLDER
401,40,1,1
```

```
*ELEMENT,TYPE=ISL21AT
501,131,132
*ELGEN,ELSET=DIE
501,50,1,1
*ELEMENT,TYPE=ISL21AT
301,301,303
311,321,322
*ELGEN,ELSET=PUNCH
301,10,2,1
311,30,1,1
*ELSET,ELSET=TOOLS
PUNCH,DIE,HOLDER
*ELSET,ELSET=ALL
BLANK,TOOLS
**
** Tool Slidelines
*SLIDELINE,ELSET=PUNCH,TYPE=LINEAR,GENERATE,SMOOTH=0.5
613,601,-1
*SLIDELINE,ELSET=DIE,TYPE=LINEAR,GENERATE,SMOOTH=0.5
501,513,1
*SLIDELINE,ELSET=HOLDER,TYPE=LINEAR,SMOOTH=0.01
404,403,402,401
**
** Define Material
*SOLID SECTION,MATERIAL=STEEL,ELSET=BLANK
*MATERIAL,NAME=STEEL
*CONDUCTIVITY
16.2
*DENSITY
7880.
*SPECIFIC HEAT
502.
*USER MATERIAL,CONSTANTS=4
200.0E9,0.29,50.0,2.0
*DEPVAR
13
*USER SUBROUTINES,INPUT=um2_rd11.f
**
** Define friction and heat generation conditions
*INTERFACE,ELSET=DIE
*GAP HEAT GENERATION
0.8
*GAP CONDUCTANCE
5000.0
*FRICTION
0.1
*INTERFACE,ELSET=HOLDER
*GAP HEAT GENERATION
0.8
*GAP CONDUCTANCE
5000.0
*FRICTION
0.1
*INTERFACE,ELSET=PUNCH
*GAP HEAT GENERATION
0.8
*GAP CONDUCTANCE
5000.0
```

```
*FRICTION
0.25
**
*INITIAL CONDITIONS,TYPE=TEMPERATURE
BLANK,20.0
**
** Tie tool nodes to one defining node for each tool
*MPC
TIE,502,501
TIE,503,501
TIE,504,501
TIE,505,501
TIE,506,501
TIE,507,501
TIE,508,501
TIE,509,501
TIE,510,501
TIE,511,501
TIE,512,501
TIE.513,501
TIE,602,601
TIE,603,601
TIE,604,601
TIE,605,601
TIE,606,601
TIE,607,601
TIE,608,601
TIE,609,601
TIE,610,601
TIE,611,601
TIE,612,601
TIE,613,601
TIE,401,403
TIE,402,403
TIE,404,403
**
** Apply prescribed holding force to the blankholder
*STEP,INC=50,AMP=RAMP,NLGEOM
APPLY THE FORCE ON THE BLANKHOLDER
*COUPLED TEMPERATURE-DISPLACEMENT,DELTMX=10.
0.01,1.,1.E-6
*BOUNDARY
CENTER,1,1
DIE,1,1
DIE,2,2
PUNCH,1,1
PUNCH,2,2
HOLDER,1,1
TOOLS,11.11,20.0
*CLOAD
HOLDER,2,-4000.
*EL PRINT,FREQ=0
*NODE PRINT,FREQ=0
*MONITOR,NODE=403,DOF=2
*END STEP
**
** Move the punch through prescribed displacement in the required time
*STEP,INC=500,NLGEOM
```

```
MOVE THE PUNCH DOWN
*COUPLED TEMPERATURE-DISPLACEMENT,DELTMX=100.
.0001,0.25,1.0E-7
*CONTROLS,ANALYSIS=DISCONTINUOUS
*BOUNDARY,OP=NEW
CENTER,1,1
DIE,1,1
DIE,2,2
PUNCH,1,1
PUNCH,2,2,-0.025
HOLDER,1,1
TOOLS,11,11,20.0
*CLOAD
HOLDER,2,-4000.
*EL PRINT,FREQ=0
*NODE PRINT,FREQ=0
*MONITOR,NODE=601,DOF=2
*END STEP
**
** Remove the tools
*STEP,INC=200,NLGEOM
*STATIC
1.,1.,1.E-6
*BOUNDARY,FIXED
BLANK,1,2
*MODEL CHANGE,REMOVE
TOOLS
*CLOAD,OP=NEW
HOLDER,2,0.
*END STEP
**
** Allow formed component to relax elastically to simulate springback
*STEP,INC=200,NLGEOM
RELAX BC'S
*STATIC
0.001,1.,1.E-6
*BOUNDARY,OP=NEW
CENTER,1,1
181,2,2
*END STEP
**
```